Anthropogenic Mixing in Seasonally Stratified Shelf Seas by Offshore Wind Farm Infrastructure

Dorrell, Rob; Lloyd, Charlie; Lincoln, Ben; Rippeth, Tom; Taylor, John ; Caulfield, Colm-Cille; Sharples, Jonathan; Polton, Jeff; Scannell, Brian; Greaves, Deborah; Hall, Rob; Simpson, John

Frontiers in Marine Science

DOI:
https://doi.org/10.3389/fmars.2022.830927

Published: 22/03/2022

Publisher's PDF, also known as Version of record

frontiers in Marine Science

REVIEW
published: 22 March 2022
doi: 10.3389/fmars.2022.830927

Anthropogenic Mixing in Seasonally Stratified Shelf Seas by Offshore Wind Farm Infrastructure

Robert M. Dorrell[1], Charlie J. Lloyd[1], Ben J. Lincoln[2], Tom P. Rippeth[2], John R. Taylor[3], Colm-cille P. Caulfield[3,4], Jonathan Sharples[5], Jeff A. Polton[6], Brian D. Scannell[2], Deborah M. Greaves[7], Rob A. Hall[8] and John H. Simpson[2]*

[1] *Energy and Environment Institute, University of Hull, Hull, United Kingdom,* [2] *School of Ocean Sciences, Bangor University, Bangor, United Kingdom,* [3] *Department of Applied Mathematics and Theoretical Physics, University of Cambridge, Cambridge, United Kingdom,* [4] *BP Institute, University of Cambridge, Cambridge, United Kingdom,* [5] *School of Environmental Sciences, University of Liverpool, Liverpool, United Kingdom,* [6] *National Oceanography Center, Joseph Proudman Building, Liverpool, United Kingdom,* [7] *School of Engineering, Computing and Mathematics, University of Plymouth, Plymouth, United Kingdom,* [8] *Centre for Ocean and Atmospheric Sciences, School of Environmental Sciences, University of East Anglia, Norwich, United Kingdom*

OPEN ACCESS

Edited by:
Frédéric Cyr, Fisheries and Oceans Canada, Canada

Reviewed by:
Andrew M. Fischer, University of Tasmania, Australia
Peter Hamlington, University of Colorado Boulder, United States

****Correspondence:***
Robert M. Dorrell
r.dorrell@hull.ac.uk

Specialty section:
This article was submitted to Physical Oceanography, a section of the journal Frontiers in Marine Science

Received: *07 December 2021*
Accepted: *24 January 2022*
Published: *22 March 2022*

Citation:
Dorrell RM, Lloyd CJ, Lincoln BJ, Rippeth TP, Taylor JR, Caulfield CCP, Sharples J, Polton JA, Scannell BD, Greaves DM, Hall RA and Simpson JH (2022) Anthropogenic Mixing in Seasonally Stratified Shelf Seas by Offshore Wind Farm Infrastructure. Front. Mar. Sci. 9:830927. doi: 10.3389/fmars.2022.830927

The offshore wind energy sector has rapidly expanded over the past two decades, providing a renewable energy solution for coastal nations. Sector development has been led in Europe, but is growing globally. Most developments to date have been in well-mixed, i.e., unstratified, shallow-waters near to shore. Sector growth is, for the first time, pushing developments to deep water, into a brand new environment: seasonally stratified shelf seas. Seasonally stratified shelf seas, where water density varies with depth, have a disproportionately key role in primary production, marine ecosystem and biogeochemical cycling. Infrastructure will directly mix stratified shelf seas. The magnitude of this mixing, additional to natural background processes, has yet to be fully quantified. If large enough it may erode shelf sea stratification. Therefore, offshore wind growth may destabilize and fundamentally change shelf sea systems. However, enhanced mixing may also positively impact some marine ecosystems. This paper sets the scene for sector development into this new environment, reviews the potential physical and environmental benefits and impacts of large scale industrialization of seasonally stratified shelf seas and identifies areas where research is required to best utilize, manage, and mitigate environmental change.

Keywords: offshore wind energy, shelf seas, marine biogeochemistry, stratification, turbulent mixing

1. INTRODUCTION

Renewable energy solutions, including offshore wind, are prerequisite for clean growth and thus the reduction of greenhouse gas emissions needed to mitigate against climate change. Offshore wind energy in shelf seas has seen a rapid increase over the past decade (Díaz and Soares, 2020; Xu et al., 2020), motivated by: high-quality and reliable energy (wind) resources (Esteban et al., 2011); space availability and site accessibility for installation of large, efficient, turbine systems (Sun et al., 2012); rapidly maturing, reliable and energy-efficient technologies (Jansen et al., 2020); and reduced visual impact on populated areas (Wen et al., 2018). Government programmes have helped drive development of renewable offshore wind energy from offshore wind farm arrays, of tens increasing

to hundreds, of offshore wind turbines (OWT) supported by various fixed foundation designs with new floating foundations being designed to access deeper water sites. Northwest Europe has led sector development, with the UK leading in gigawatt (GW) operational capacity to date (Global Wind Energy Council, 2020). The sector has grown rapidly, with technological advances reducing the Levelised Cost of Electricity to a point where price is competitive with alternative energy solutions (Shen et al., 2020). Thus, to meet demand, global development of offshore wind energy in shelf seas is predicted to grow from 35 GW operational in 2020 to 243 GW operational by 2030 (**Figure 1A**).

With over 80% of the global population living within 100 km of the ocean, shelf seas have significant economic and social value, including fishing, shipping, carbon storage ("blue" carbon) and recreation. Despite comprising 8% of the total area of the global ocean (**Figure 1A**), shelf seas support 15–30% of global ocean biological production (Wollast, 1998). This biological production ultimately supports > 90% of the world's fish landings (Pauly et al., 2002) and plays a disproportionately important role in the absorption of CO_2 from the atmosphere (Roobaert et al., 2019). Thus, high biological productivity means shelf seas are key components of global biogeochemical cycles, supporting societally important bioresources and also the biological uptake and storage of carbon in the marine environment. However, interplay of social and economic drivers already places significant stress on shelf seas (Kröger et al., 2018). Further industrialization of shelf seas will enhance these stresses, with the potential for significant long term environmental impact. Shelf sea dynamics directly control primary production: the growth of microscopic marine plankton. However, from OWT scale to coastal scale, the impact of offshore wind development on shelf seas has yet to be fully considered. Therefore, future offshore wind energy development must be grounded in advanced understanding of impact on shelf sea dynamics. This is critical to enable balance of key global societal goals, i.e., to ensure access to affordable, reliable, sustainable and modern energy and to conserve and sustainably use the oceans, seas and marine resources (United Nations, 2015).

To date, most offshore wind farms have been installed in the near-shore shallow water regions, up to 50 m depth, of shelf-seas (**Figure 1B**). Near-shore shallow-water installations have been preferred due to the cost reduction from ease of access for installation, grid connection and operation and maintenance (Jacobsen et al., 2019). With sector plans for an additional 208 GW of operational capacity in the next decade, and targets of 1.4 TW total by 2050 (Offshore Renewable Energy Action Coalition, 2020), near-shore and shallow-water sites are rapidly becoming limited. The scale of expansion of offshore wind energy means the sector is now expanding into deeper water sites further from shore (Soares-Ramos et al., 2020). The transition from near-shore and shallow-water environments to deeper water further from shore marks a fundamental change in the marine environment. Shallow waters are typically well-mixed; however deeper waters may be subject to seasonal stratification, where density varies vertically with depth (**Figures 1A,B**). Stratified waters are a vital part of shelf seas, controlling primary production and biogeochemical cycling (Simpson and Sharples, 2012). Expansion into this new environment means that offshore wind farms will increasingly come into conflict with its environmental functioning, controlled by natural mixing of water column stratification (**Figure 1C**).

Addressing engineering challenges, both fixed and floating foundations are being developed to enable expansion into deeper waters. Fixed foundations, which span the entire water depth, include monopiles, gravity bases and jacket constructions (see, e.g., **Figure 2** and Esteban et al., 2019; Díaz and Soares, 2020; Jiang, 2021b). However, floating foundations are crucial to deep water, > 50 meters, deployment. Learning from the petroleum industry (Schneider and Senders, 2010), designs include tension-leg platforms (Uzunoglu and Soares, 2020), spar-pendulum (Cottura et al., 2021) and spar-buoy platforms (Jacobsen and Godvik, 2021), and semi-submersible platforms (Castro-Santos et al., 2020). Using the submerged structural buoyancy and mooring forces to balance atmospheric thrust and wave loads, floating foundations typically have large draft, e.g., spar platforms, or large cross sectional area, e.g., semi-submersible platforms (Butterfield et al., 2007). Thus, with sector development requiring larger turbines that need bigger rotors, which are subject to greater atmospheric loads, the draft and diameter of fixed and floating foundations will need to increase. The dynamics of atmospheric wakes from OWT are already of key interest, given their control on available wind power from turbine to array scale (Howland et al., 2019). However, the dynamics of sub sea surface wakes from foundations in well-mixed, and in particular, stratified waters is poorly understood. Despite this, the > 20 m minimum draft of current floating foundations is already large enough to penetrate the thermocline and directly mix seasonally stratified shelf seas (**Figure 2**).

For the first time, large scale industrialization of seasonally stratified marine environments is planned. Over two decades of research has already focused on the direct impacts of offshore wind farm development on well-mixed shallow water marine ecosystems, from: benthic habitats (Dannheim et al., 2020), fisheries (Gray et al., 2005) to seabirds (Exo et al., 2003). Whilst this research is translatable with sector growth, the seasonally stratified regime offers a fundamentally new challenge: the introduction of infrastructure will lead to enhanced "*anthropogenic*" mixing of stratified waters. Enhanced mixing may lead to profound impacts on shelf sea dynamics and thus marine ecosystem functioning. The aim of this paper is to investigate the scope of these potential impacts. Section 2 reviews the ecosystem and physical functioning of stratified shelf seas, highlighting the interface of physical and biogeochemical processes where offshore wind farm scale and submesoscales coincide. Section 3 then describes our current understanding of the impact of offshore infrastructure on unstratified and stratified waters. Section 4 discusses current research challenges, the potential impact of offshore wind on stratified shelf seas and the sector requirements needed to ensure acceleration of renewable energy and its sustainable development. It is concluded that offshore wind farm infrastructure may have significant, and long lasting, effects on

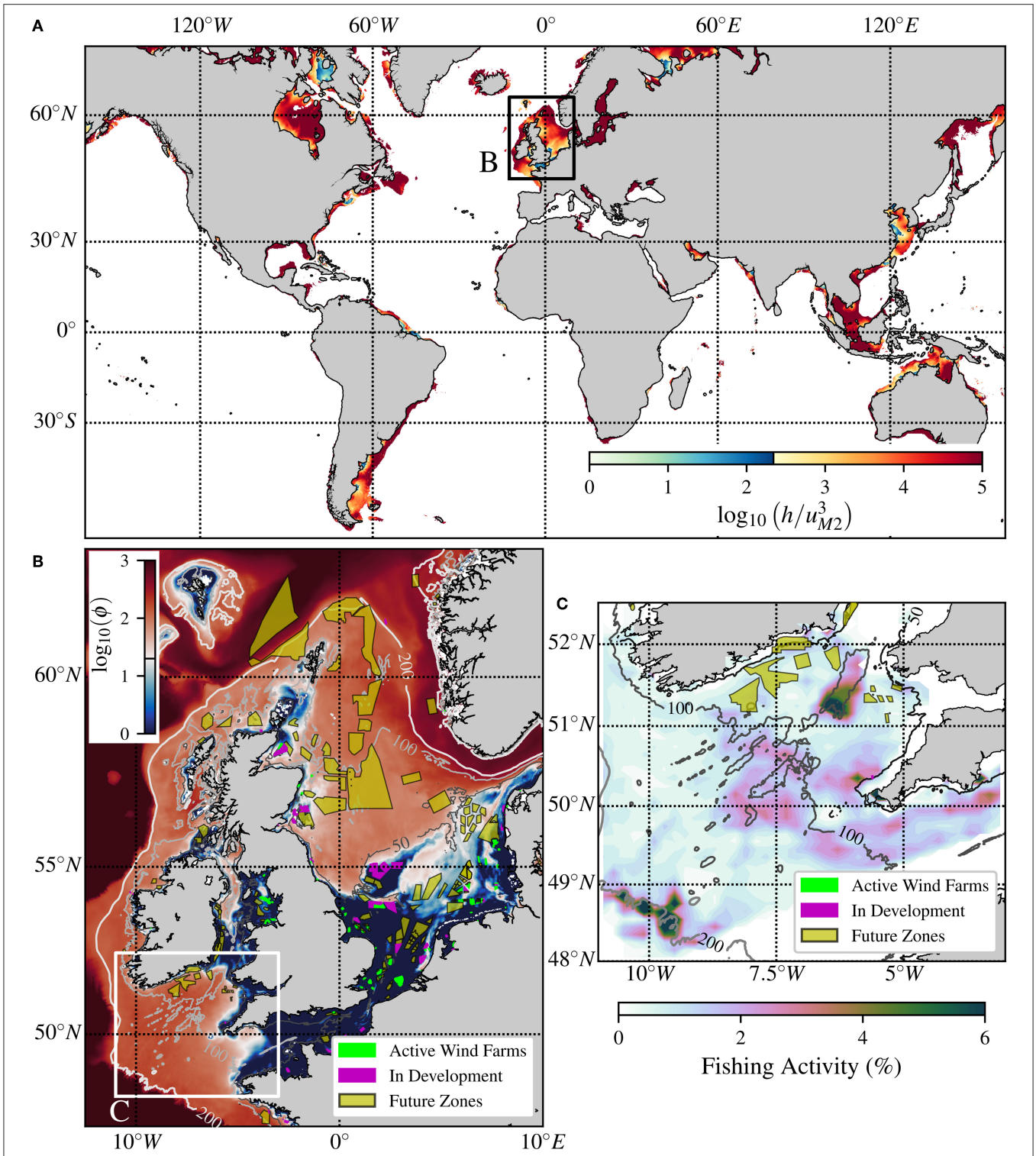

FIGURE 1 | Offshore wind and seasonally stratified shelf seas. **(A)** Shelf sea development; the limited extent of well-mixed waters, defined using the "h/u_{M2}^3" criterion, is highlighted against projected global offshore wind energy growth (Global Wind Energy Council, 2020). **(B)** NEMO model of the Northwest Europe summer potential energy anomaly, ϕ, a measure of the amount of stratification (Guihou et al., 2018). **(C)** Fishing hotspots in the Celtic sea caused by topographically-enhanced mixing of stratified waters (Sharples et al., 2013). In **(A,B)** seas are partitioned into regions prone to seasonal stratification and those remaining well mixed, based on: **(A)** $h/u_{M2}^3 = 220\,\mathrm{s^3\,m^{-2}}$ (Simpson and Sharples, 2012); and **(B)** $\phi = 20\,\mathrm{J\,m^{-3}}$ (Gowen et al., 1995). In **(B,C)** offshore wind farms are separated into active sites, sites still in construction or development and identified zones for future development (4C Offshore, 2021).

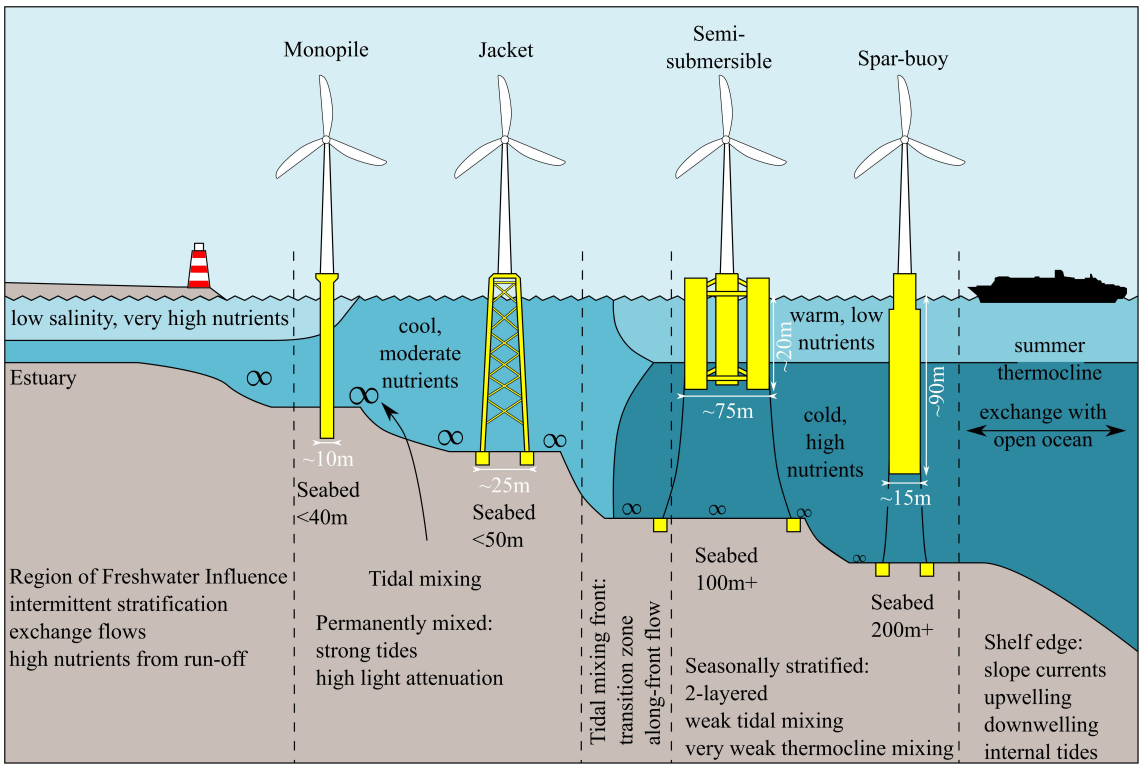

FIGURE 2 | Existing and emerging offshore wind engineering solutions (Díaz and Soares, 2020; Jiang, 2021b), including fixed monopile and jacket foundations and floating semi-submersible and spar-buoy foundations, in comparison to shelf sea regimes from coastline to open ocean (Simpson and Sharples, 2012).

fragile shelf sea ecosystems. Criteria for Environmental Impact Assessments, must therefore be revised and updated to enable the sustainable growth, and acceleration, of renewable offshore wind energy development.

2. OCEANOGRAPHY OF STRATIFICATION IN SHELF SEAS

Shelf seas lie on the continental shelf between the coast and the continental slope, where at 200 m water depth the sea floor slopes down to the deep ocean. Despite only accounting for 0.5% of ocean volume shelf seas play a key role in the Earth system, dissipating > 70% of the tidal energy (Egbert and Ray, 2000) and are disproportionately important in supporting ocean biological production (Wollast, 1998), fish landings (Pauly et al., 2002) and the absorption of CO_2 from the atmosphere (Roobaert et al., 2019). Biological production is underpinned by the growth of microscopic marine phytoplankton, which is tightly controlled by the timing and strength of seasonal stratification. The seasonally stratified zones in shelf seas act as an important net sink of carbon (Thomas et al., 2004). This makes the physical and biogeochemical processes described here a key dynamic component of the global carbon cycle (Bauer et al., 2013) linking the atmospheric, terrestrial, and oceanic carbon pools.

2.1. Distribution and Seasonal Cycle of Stratification

The focus of offshore wind development is now shifting to the central regions of temperate shelf seas; away from the generally tidally energetic coast, and regions of freshwater influence (**Figure 1B**). In these central shelf-sea regions the water column structure of temperate shelf seas undergoes a seasonal cycle in response to changes in heat exchange at the surface. In spring and summer, some areas of the temperate shelf seas become thermally stratified whilst neighboring areas remain well mixed. Here it has been established that the first order control on the water column structure is the balance between the stratifying influence of surface heating and turbulent mixing due to the tides (Simpson and Hunter, 1974; Holt and Proctor, 2008). Within the regions of seasonal stratification the energy sources and pathways to mid-water column mixing remains an area of active research (Lincoln et al., 2016; Inall et al., 2021). In regions of shallow water and strong tidal currents (of order meters per second), the rate of buoyancy input due to surface heating is insufficient for the establishment of persistent stratification, and in consequence the water column remains homogeneous. However, in regions of deeper water and/or weaker tidal currents (and associated lower levels of turbulence), surface heating dominates and seasonal stratification develops. Away from coastal regions, shelf seas generally exhibit tidal currents of order of tens of cm per second, meaning that stratification are typically found when water depths

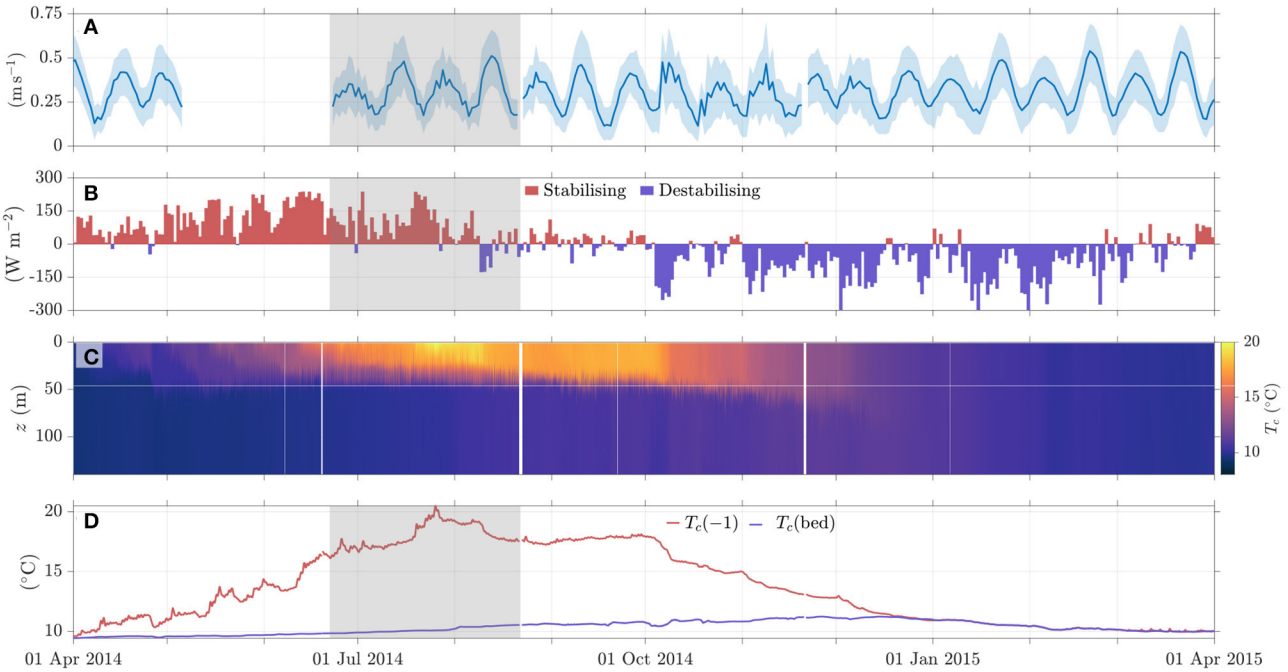

FIGURE 3 | Seasonal time-series of mooring observations from 2014 in the Celtic Sea (49°24 N 8°36 W), collected as part of the UK Natural Environment Research Council (NERC) funded CaNDyFloSS project (NE/K00168X/1) (Scannell, 2020). **(A)** Measured thermocline current speed over 20–50 m mean depth; average speed (blue line) and range (shaded region) over 2 tidal periods. **(B)** Surface heat exchange. **(C)** Vertical temperature structure. **(D)** Surface and bottom layer temperatures.

are greater than 80 m. In stratified regions, a warmer surface water layer 5–40 m thick overlies a deeper cooler water layer. The two layers are separated by a region of strong vertical temperature gradient, the thermocline, which forms a barrier to vertical exchange of heat, salt, nutrients and momentum.

Tidal mixing fronts separate regions of seasonal stratification from well mixed regions. Simpson and Hunter (1974) use an energetics argument to derive a single parameter to predict the positions of these fronts. By considering only vertical exchange processes and assuming the surface input of heat was the only stratifying influence, and that tidal currents are the only source of energy driving mixing, they showed that the first order determinate for the position of shelf sea fronts is given by the ratio

$$\frac{h}{u_{M2}^3}, \tag{1}$$

where u_{M2}^3 is the principle lunar M2 tidal current amplitude, and h is water depth (**Figure 1A**). In **Figure 1A** h/u_{M2}^3 is calculated from bathymetry and M_2 tide data taken from TPX09 global tidal atlas (Egbert and Erofeeva, 2002), which applies a generalized inverse method, assimilating satellite altimeter data, into a global barotropic tidal model; here model resolution limits precise location of stratified fronts from global data. In terms of area, regions of seasonal stratification dominate the continental shelf seas (**Figure 1A**). Whilst the critical value for the ratio characterizing the position of tidal mixing fronts was initially estimated for the Irish Sea (Simpson and Hunter, 1974; Simpson and Bowers, 1981), consistent values have continued to be estimated for a range of shelf seas globally. Examples include the Gulf of Maine and Bay of Fundy, Garrett et al. (1978) and Loder and Greenberg (1986); the South China (Tong et al., 2010) and Yellow Sea, Lie (1989) and Ren et al. (2014); the Patagonian Shelf, Glorioso and Flather (1995); the northwest European Shelf Seas, Pingree and Griffiths (1978), Sheehan et al. (2018) and the Bering Sea, Schumacher et al. (1979). The robustness of the critical value highlights the key role of the tides in determining the position of shelf sea fronts and provided the first quantitative link between the dissipation of tidal energy and ocean mixing.

The strength of stratification may be quantified in terms of the potential energy anomaly, ϕ (J m^{-3}), which describes the energy required to fully mix a stratified water column (Simpson and Bowers, 1981),

$$\phi = \frac{g}{h}\int_{-h}^{0}(\overline{\rho} - \rho)z dz, \tag{2}$$

where h is the water depth and ρ the water density, $\overline{\rho}$ denotes the density calculated using the mean water temperature and salinity (Holt and Proctor, 2008). Geographical variation of ϕ across the NW European Shelf Seas is plotted on the map in **Figure 1B**.

A typical seasonal stratification cycle shows a time-series of warming and cooling, varying with water depth (**Figure 3**). Surface mixed layer temperatures warm from April into the summer in response to a net positive buoyancy input due to surface heating. The observed surface temperatures of $15-20$ °C are typical for temperate shelf seas in midsummer, while the deep

water remains close to its winter temperature of 10 °C. Over this period the strength of stratification grows with a surface to bed temperature difference exceeding 10 °C by August, which gives rise to a density difference of 0.3 kg m^{-3}. The stratification weakens into autumn as surface cooling leads to convection and storms drive turbulent mixing, such that the water column becomes well mixed during the winter.

During the stratified period the deeper water is isolated from the surface layer by a thermocline. A slow warming of the deep-water results from mixing down of heat from the sea surface. The rate of warming, set by thermocline mixing, varies geographically and is important as it determines the timing of the autumnal breakdown of stratification (Rippeth, 2005), and transport of nutrient rich deep water up to the surface layer.

Regional variations on controls of the distribution, and seasonal cycles of stratification, do exist. For example, wind driven upwelling on narrow shelves, subject to weak tides, can dictates patterns of stratification (see, e.g., Austin and Barth, 2002). However, offshore wind sector development has not yet extended to such regions.

2.2. Ecosystem Response to Stratification

Primary production of organic matter by phytoplankton forms, directly or indirectly, the primary food source for almost all marine organisms. Phytoplankton growth requires CO_2, sunlight and nutrients, the availability of which are determined by water column structure, with profound implications for the biological functioning of the shelf seas.

In turbulent unstratified regions, primary production occurs mainly during summer months when sunlight is strong. However, plankton are continuously mixed from sea surface to bed by turbulence, and spend much of their time below a depth where light intensity is sufficient for growth. In contrast, stratified waters provide ideal conditions for phytoplankton growth in spring. As stratification forms phytoplankton become trapped in the well lit surface layer, with the thermocline acting as a barrier to mixing. Phytoplankton retained in the surface layer enjoy the abundance of light, and exhibit rapid growth forming the annual "spring bloom," a biological abundance visible from space that forms the year's first supply of significant new organic fuel. As the phytoplankton grow, they fix inorganic carbon in the surface water into organic carbon, which causes the sea surface to replenish its dissolved carbon concentration by absorbing CO_2 from the atmosphere. The timing of the spring bloom is so significant that zooplankton and fish larvae have evolved to use it as a food source (Platt et al., 2003), with further implications higher up the food-web, e.g., for shrimp survival (Ouellet et al., 2011) and seabird breeding success (Frederiksen et al., 2006).

During the spring bloom, the availability of nutrients in the surface layer becomes exhausted, and further production is limited by nutrient supply. Despite this limitation on plankton growth, a persistent and significant level of primary production is sustained at depth, throughout the period of seasonal stratification. This sub-surface phytoplankton layer located in the stratified thermocline water is a ubiquitous feature and is known as the "subsurface chlorophyll maximum" (SCM) (Pingree et al., 1982). In shelf seas, the SCM occupies a 10–30 m thick layer, the depth of which varies from 10 to 40 m across the hundreds of kms that it extends over the shelf (**Figure 4**). The SCM plays a vital role in supporting the pelagic food web during summer. Estimates based on observations of primary production rates within the SCM suggest that subsurface carbon fixation accounts for up to 50% of annual primary production in the seasonally stratified North Sea (Richardson et al., 2000; Weston et al., 2005). An extrapolation using microstructure-based nitrate flux estimates also gives the same approximate figure (Rippeth et al., 2009). The persistence of production in the SCM is dependent on a vertical flux of nutrients from the deep nutrient-rich water below (Sharples and Tett, 1994). In consequence, the processes responsible for mixing across the thermocline, discussed in Section 2.5, are key to delivering the limiting nutrients to the euphotic zone and sustaining the SCM (Sharples et al., 2001a,b, 2007; Williams et al., 2013a). Episodic mixing associated with storm initiated inertial oscillations (Burchard and Rippeth, 2009; Lincoln et al., 2016) have been shown to drive significantly enhanced nutrient fluxes (Williams et al., 2013b). Local enhancement of primary productivity is evident in regions of steep topography, where tidally induced internal waves elevate mixing and nutrient fluxes. Chlorophyll concentration in the SCM is greatly elevated at the shelf break (Sharples et al., 2007), and mid-shelf sand banks (Sharples et al., 2013). The dependence of the marine food web and fisheries on upward flux of nutrients is evident in the distribution of seasonal fishing hot-spots (**Figure 1C**).

The organic products of the spring and summer primary production sink into the deeper waters, where bacteria remineralise the organic material (nutrients and carbon) back to the inorganic components. Remineralisation removes oxygen from the deep water. In addition, the barrier role of the thermocline limits the replenishment of that oxygen from the atmosphere (Mahaffey et al., 2020). Together both processes determine the dissolved oxygen concentrations available to benthic and pelagic organisms. Thus, high shelf sea biological productivity means shelf seas are key components of global biogeochemical cycles, supporting societally important bioresources, and also the biological uptake and storage of carbon in the marine environment.

2.3. Shelf Sea Mixing Processes

Currents in shelf seas provide energy for stirring the water column and are generally dominated by tidal motions, with episodic contributions by the wind in the upper water column. An example of the current variability from the Celtic Sea, a typical shelf sea location, is presented in **Figure 3A**, where velocities vary from 0.1 to 0.7 m s^{-1}. For this location, the semi-diurnal tide lunar M_2 produces two high and low tides a day with 4 peaks in current speed. The interaction with the principle solar tidal component, S_2, produces the 14 day spring-neap cycle. Wind driven currents are also observed in the top 50 m, and take the form of inertial oscillations, which have a latitude dependent period, which is 14.9 h at the mooring location.

Friction at the seabed and the sea surface generate vertical current shear in the flow, and turbulent eddies which cascade to

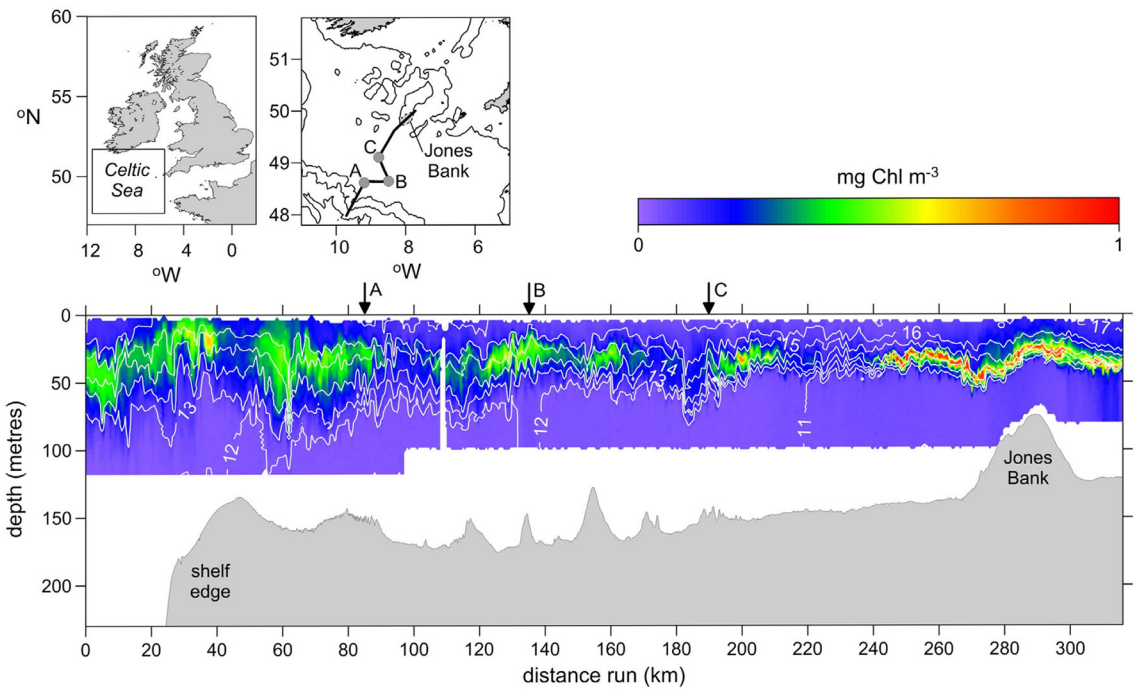

FIGURE 4 | Observational data from the Celtic Sea collected in summer 2008, supported by NERC's Oceans2025 Programme (Sharples et al., 2013). Section of temperature (line contours) and chlorophyll concentration (colors) measured using a Scanfish CTD towed along the path show on the map. High chlorophyll concentration in the SCM (subsurface chlorophyll maximum) indicate phytoplankton production extending hundreds of kms across the shelf. Enhancements in concentration over rough topography, such as Jones Bank, are a result of elevated turbulent mixing, driving nutrient fluxes which correspond directly to hotspots of marine biodiversity and thus fisheries (**Figure 1C**).

ever smaller scales until their energy is dissipated either to heat, or to potential energy via mixing.

In the absence of convection, a three-way local balance is assumed (assuming both at least quasi-stationarity and that transport terms can be ignored):

$$\mathcal{P} = \mathcal{B} + \varepsilon, \tag{3}$$

where $\mathcal{P}$ is the (total) production of turbulent kinetic energy (TKE), $\mathcal{B}$ is the buoyancy production (mixing), and ε is the TKE dissipation rate (heat).

The efficiency of mixing by turbulence can be quantified by the flux Richardson number $Rf = \mathcal{B}/\mathcal{P}$ and is widely assumed to have a value $Rf \ll 1$ in a stratified fluid. Since ε is a commonly measured turbulence metric, it is often used to infer the rate of mixing using the closely related flux dissipation coefficient, defined in terms of the buoyancy production as $\Gamma = \mathcal{B}/\varepsilon$. A value of $\Gamma \approx 0.2$ (i.e., $Rf \approx 1/6$) is routinely applied, and has been verified for the shelf sea thermocline by a number of different observational approaches (Inall et al., 2000; Oakey and Greenan, 2004; Palmer et al., 2008; Bluteau et al., 2013), though it has been found to vary in other regimes (Monismith et al., 2018).

A consequence of shear production at the seabed by barotropic tidal currents is that measured rates of turbulence are extremely low in the seasonal thermocline, orders of magnitude lower than at the boundaries (**Figure 5B**). Mean dissipation rates range from $\varepsilon = 10^{-7} - 10^{-5}$ W m^{-3} (Rippeth, 2005), 2–3 orders of magnitude smaller than rates commonly found in shallow well mixed waters (Simpson et al., 1996). Empirical estimates of the bulk mixing efficiency of the barotropic tide in stratified waters, are very low, $Rf_{BT} \approx 0.0037$ (Simpson et al., 1978), as most turbulence is produced in the well mixed bottom layer, so that no mixing is possible. In addition, strong density gradients in the thermocline inhibit vertical mixing, and as such rates of vertical mixing observed in shelf seas are comparable to using a hand mixer in a swimming pool.

The production of turbulence in stratified waters is inhibited by buoyancy forces arising from vertical density gradients, which are quantified by the Brunt-Väisälä, or buoyancy, frequency, N, where

$$N = \sqrt{-\frac{g}{\rho}\frac{\partial \rho}{\partial z}}, \tag{4}$$

describes the frequency at which a displaced parcel of fluid will oscillate in a stratified system and is thus a measure of the stability of stratified waters. Conversely, the vertical current shear, $S = \partial u/\partial z$, is a measure of the extraction of energy from the mean flow, and therefore power available to overcome buoyancy forces and generate turbulence. The generation of instabilities in stratified water is quantified using measurements of the buoyancy

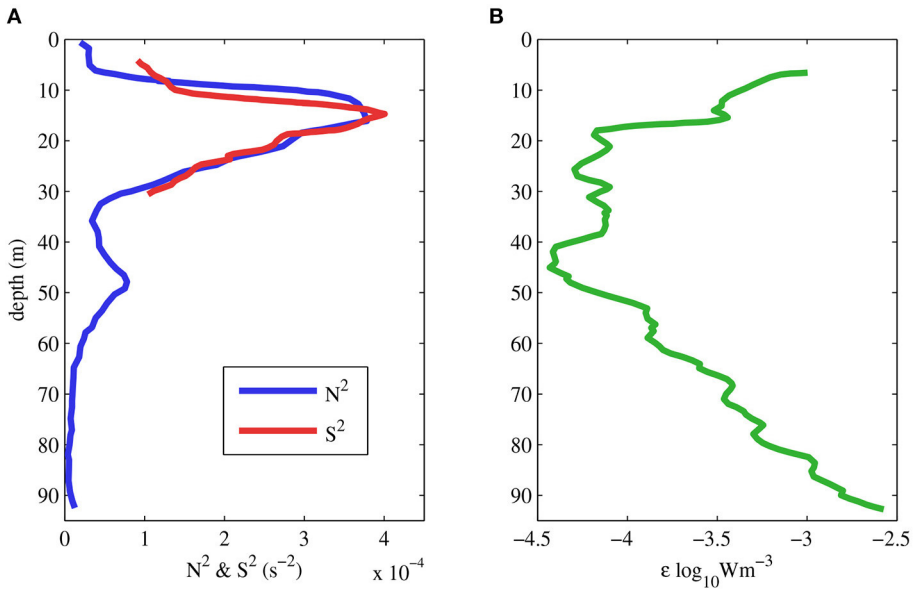

FIGURE 5 | Marginal stability and energy dissipation in seasonally stratified shelf seas. **(A)** The equivalence between buoyancy frequency N^2 (blue) and vertical current shear S^2 (red), temporally averaged (over two tidal cycles). **(B)** The coincident temporally averaged profile of TKE dissipation rate ε. Measurements from direct observations in the Western Irish Sea in June 2002 (Rippeth, 2005).

frequency, N, and vertical current shear, S, to calculate the gradient Richardson Number

$$Ri_g = -\frac{g}{\rho}\frac{\frac{\partial \rho}{\partial z}}{\left(\frac{\partial u}{\partial z}\right)^2} \equiv \frac{N^2}{S^2}. \quad (5)$$

Both theory (Howard, 1961; Miles, 1961) and observations (Silvester et al., 2014; Lincoln et al., 2016) show that shear instability and internal wave breaking occurs when $Ri_g \lesssim 0.25$. Average of measurements, over two tidal cycles, show N^2 and S^2 are approximately equal implying a (close to) marginally stable water column where $Ri_g \approx 1$ (**Figure 5A**). Therefore, any additional sources of shear can generate instabilities and mixing. This marginal stability has been widely observed across shelf seas (van Haren et al., 1999; Rippeth, 2005; Palmer et al., 2008) but it does not universally explain the observations (Palmer et al., 2013) suggesting additional sources of shear may, at times, control system dynamics.

One dimensional vertical exchange models using turbulence closure schemes (also commonly referred to as RANS models) fail to represent the measured rates of mixing through tidal and wind driven boundary processes (Simpson et al., 1996). The deficit in the predicted mid-water ε points to either an incorrect parameterisation of the small scale physics away from the boundaries or to the absence of key physical processes in the model. A recent study (Luneva et al., 2019) evaluated a range of alternative one dimensional turbulence closure schemes for the Northwest European shelf seas, packaged within the Generic Length Scale two-equation formulation (Umlauf and Burchard, 2005). Evaluating the schemes against profile data (28,000 profile in total) confirmed that there was no outright winner, with all schemes under representing the thermocline properties and suggested that physical processes are still missing. Candidate mechanisms to account for the deficit in mid water mixing include internal waves generated by stratified flow over topography and wind generated inertial currents.

Internal tides propagate at the thermocline in response to tidal currents flowing over steep topography (Rippeth, 2005; Inall et al., 2021). These waves generate strongly sheared currents about the thermocline which can lead to the development of shear instability, draining energy to turbulence which then supports mixing in the quiescent mid-water region. Although the energy in the internal tide is much less than the barotropic tide, an empirical estimate of bulk mixing $Rf_{IT} \approx 0.056$ (Stigebrandt and Aure, 1989) shows it to be highly efficient compared with the barotropic tide $Rf_{BT} \approx 0.0037$ (Simpson et al., 1978), on account of the turbulence coinciding with the stratification. A consequence of the differing bulk mixing efficiencies is that whilst the barotropic tide dominates the budget for the dissipation of barotropic tidal energy in the seasonally stratified shelf seas to the west of the UK, the shelf break generated internal tide is estimated to dominate diapcynal mixing (Rippeth et al., 2005). With advances in computational performance and associated resolution increase, simulation of internal tides are now routine for European Shelf simulations (Guihou et al., 2018) implemented operationally (Graham et al., 2018; Tonani et al., 2019). Though, as hydrostatic simulations, the non-hydrostatic mixing processes must still be parameterised.

2.4. Submesoscale Mixing

The size of many existing and proposed offshore wind farms coincides with the ocean submesoscale ($\sim 1 - 20$ km). The

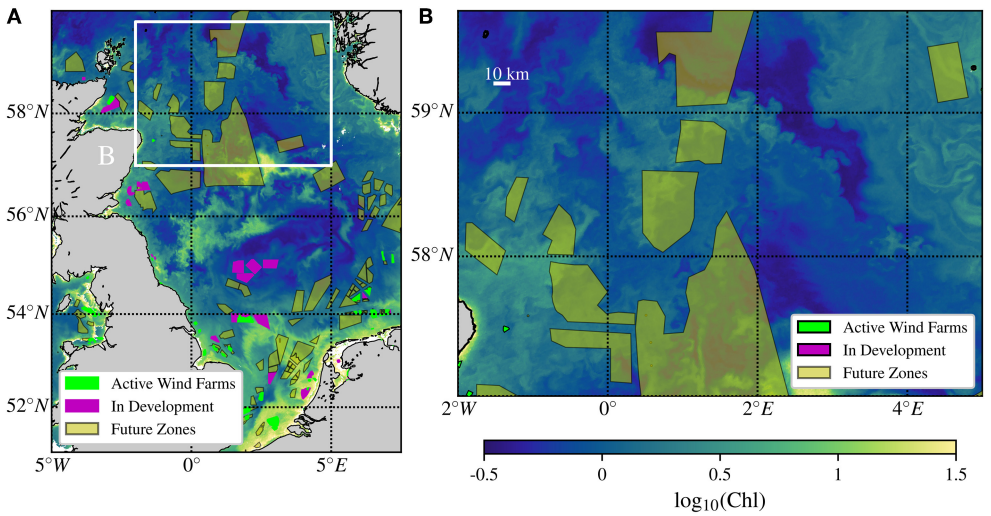

FIGURE 6 | Near-surface chlorophyll concentration (mg m^{-3}) from 20 April, 2020, inferred from the NASA MODIS Aqua satellite. **(A)** Chlorophyll concentration for Northwestern European waters. **(B)** Detail of the north North sea highlighting submesoscale instabilities at, and below, the scale of offshore wind farm development. The image was made from data downloaded from http://oceancolor.gfsc.nasa.gov and 4C Offshore (2021).

imprint of submesoscale eddies can be seen in satellite images of chlorophyll concentration in the North Sea as seen in **Figure 6** (note that the future development zones shown for reference will likely consist of multiple smaller windfarms). The submesoscale range is characterized by Rossby numbers, $Ro \equiv u/(fL) \sim 1$, where u and L are characteristic horizontal velocity and length scales associated with submesoscales and f is the Coriolis parameter. This makes submesocales dynamically distinct from mesoscales ($\sim$ 100 km) where $Ro \ll 1$. While the Earth's rotation is important on submesoscales, it does not constrain the flow as strongly as it does for larger scales, leading to a unique set of physical processes. Submesoscale currents are generally more energetic in regions with large horizontal density contrasts which includes coastal waters.

It is not clear if, or how, offshore wind farms might interact with submesoscale currents. However, since the spatial extent of wind farms typically lie within the submesoscale range, array scale flow patterns generated by enhanced drag or mixing within offshore wind farms could be subject to the physical processes that are active on the submesoscale. Below we very briefly consider some of these processes. See Thomas et al. (2008), McWilliams (2016), and Gula et al. (2022) for in-depth reviews of submesoscale dynamics.

Submesoscales are typically generated by dynamical instabilities or flow/topography interactions. The instability mechanisms include ageostrophic versions of instabilities that also exist at larger scales (e.g., baroclinic instability) and instabilities that are unique to the submesoscale (e.g., inertial/centrifugal and symmetric instability). Although the details and energy pathways differ, the net effect of submesoscale instabilities is to convert potential energy associated with horizontal density gradients into kinetic energy. In the process, submesoscales increase the water column stratification and tend to reduce the depth of the surface mixed layer. Submesoscales can also be generated as currents move around topographic features. For example, submesoscale eddies can be generated by flow past islands (Marmorino et al., 2018), along continental slopes (Gula et al., 2015; Molemaker et al., 2015), and over seamounts (Srinivasan et al., 2019). It is possible that the enhanced drag experienced by the flow through a submesoscale offshore wind farm could similarly generate submesoscale eddies. The enhanced mixing and drag within wind farms could also influence submesoscale instabilities and eddies, although these hypotheses remain untested.

Submesoscales are important partly because they interact with vertical mixing processes. Submesoscales are characterized by timescales that range from hours to $\sim$ 1 day. As a result, the tendency for submesoscales to increase the vertical stratification of the water column is fast enough to compete with vertical mixing driven by winds and tides. At the same time, submesoscales can induce strong vertical circulations and locally enhance the exchange between the surface mixed layer and thermocline (Mahadevan and Tandon, 2006). Gula et al. (2015) provide an in-depth review of the connections between submesoscales and ocean mixing.

Submesoscales can have a strong impact on biogeochemistry (Lévy et al., 2012; Mahadevan, 2016). For example, shoaling of the surface mixed layer depth and suppression of turbulent mixing induced by submesoscales can trigger phytoplankton blooms in otherwise light-limited conditions (Taylor and Ferrari, 2011; Mahadevan et al., 2012; Taylor, 2016). In nutrient-limited conditions, submesoscales can upwell nutrient-rich waters to the euphotic zone, enhancing primary production (Mahadevan and Archer, 2000; Lévy et al., 2001). Finally, downwelling circulation and the suppression of turbulent mixing can enhance the export

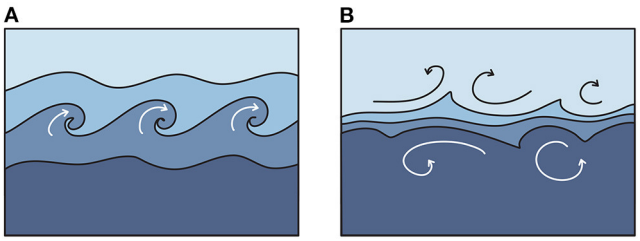

FIGURE 7 | Cartoon illustrating overturning **(A)** and scouring **(B)** regimes at a density interface (Caulfield, 2021).

of particulate organic matter from the surface mixed layer (Omand et al., 2015; Taylor et al., 2020).

2.5. Mixing Across Density Interfaces

As noted, stratified shelf seas sometimes exhibit a two-layer density structure with relatively homogeneous mixed layers at the top and bottom separated by a stratified thermocline (**Figure 3**). There are two paradigms for mixing, at the small scales of density interfaces; 'scouring' and 'overturning' (see Caulfield, 2021 and references therein). The mixing across the density interfaces and the ultimate fate of the density interface depends strongly on which regime the turbulence is in. The mixing regimes are controlled by the relative strength of stratification and turbulence. This can be quantified by the kinetic energy associated with three-dimensional turbulent eddies and the potential energy associated with the density interface. When the stratification at the density interface is sufficiently strong, turbulent eddies do not have kinetic energy to overturn the density interface. Instead, if there is a source of turbulence in the surrounding mixed layers, turbulent eddies will 'scour' the density interface, pulling characteristic wisps of fluid into the mixed layers (**Figure 7B**). On the other hand, when the kinetic energy associated with the turbulent eddies is large enough, turbulence is able to 'overturn' the density interface (**Figure 7A**).

The fate of the density interface is intimately tied to the mixing regime; scouring tends to sharpen density interfaces, while overturning tends to mix the interface into a more diffuse state. The mixing regime can be quantified by considering the budget for the buoyancy frequency in sorted density coordinates (Taylor and Zhou, 2017; Zhou et al., 2017):

$$\frac{\partial N_*^2}{\partial t} = \underbrace{\frac{\partial^2 \kappa_e}{\partial z_*^2} N_*^2}_{A} + \underbrace{2\frac{\partial \kappa_e}{\partial z_*}\frac{\partial N_*^2}{\partial z_*}}_{B} + \underbrace{\kappa_e \frac{\partial^2 N_*^2}{\partial z_*^2}}_{C}. \tag{6}$$

Here z_* is the height of a vertically sorted isopycnal, adiabatically sorted to monotonically decrease with depth; N_*^2 is the buoyancy frequency, Equation (4), in sorted height coordinates; and ρ is the potential density, where ρ_0 is a reference density. The 'effective' diffusivity is (Nakamura, 1996; Winters and D'Asaro, 1996)

$$\kappa_e = \kappa \left(\frac{\partial z_*}{\partial \rho}\right)^2 \left\langle |\nabla \rho|^2 \right\rangle_{z_*}, \tag{7}$$

where κ is the molecular diffusivity and $\langle \cdot \rangle_{z_*}$ denotes a spatial average for a fixed z_*. Note that this formulation assumes that density is controlled by one variable (temperature or salinity). The key advantage of using sorted height coordinates is that κ_e is strictly positive. A purely laminar flow has $\kappa_e = \kappa$, and turbulence will lead to $\kappa_e > \kappa$ by distorting the isopycnals, increasing the density surface and thereby increasing the density gradients.

The relative sizes of the terms on the right hand side of Equation (6) can be used to diagnose the mixing regimes. Terms B and C in Equation (6) represent translation and diffusion of the sorted density profile, respectively, and since $\kappa_e > 0$ this diffusion acts to spread out density interfaces. Term A in Equation (6) can be positive or negative, and this term dictates whether turbulence at a density interface is in the scouring or overturning regimes. For example, consider a flow in the overturning regime where shear-driven turbulence is generated at a density interface (**Figure 7A**). If the flow above and below the interface is relatively quiescent, κ_e could exhibit a local maximum at the density interface with $\partial^2 \kappa_e / \partial z_*^2 < 0$. In this case term A will act to reduce the stratification at the interface. On the other hand, in the scouring regime (**Figure 7B**) strong stratification will suppress mixing at the interface where κ_e will be relatively small. In this case strong mixing on either side of the density interface can result in a flow with $\partial^2 \kappa_e / \partial z_*^2 > 0$, in which case term A will act to increase N_*^2 and *sharpen* the interface.

The scouring regime requires a source of turbulence external to the density interface. In natural stratified shelf seas, turbulence generated by bottom friction and surface forcing (e.g., wind, waves, and/or convection) generate turbulence below and above mid-water density interfaces. Turbulence associated with flow past OWTs could also play this role. Indeed, as discussed in Section 3.2, horizontal shear can be very effective at generating and maintaining layers in stratified flows. On the other hand, energetic turbulence driven by the flow past OWTs could be strong enough to overturn and mix natural density interfaces.

Thus, it is not clear whether OWTs would generate turbulence in the overturning or scouring regime. The distinction will likely depend on the strength of stratification, the speed of flow through offshore wind farms, and the geometry of wind turbines. As will be expanded on in the following section more research is needed to understand mixing generated by offshore wind infrastructure and their impact from the scale of OWTs to the shelf sea scale.

3. FLOW STRUCTURE INTERACTIONS

The dynamics of flows past a range of structures has seen significant research over the last 50 years, both due to immediate real-world applications and the increase in computational resources and experimental measurement fidelity (Williamson, 1996). Here work studying the dynamics of unstratified and stratified flow past infrastructure, relevant to the offshore wind sector, are integrated and reviewed.

3.1. Unstratified Flow

Flows past cylindrical structures are well studied, owing to their geometrical simplicity and vast engineering importance; such

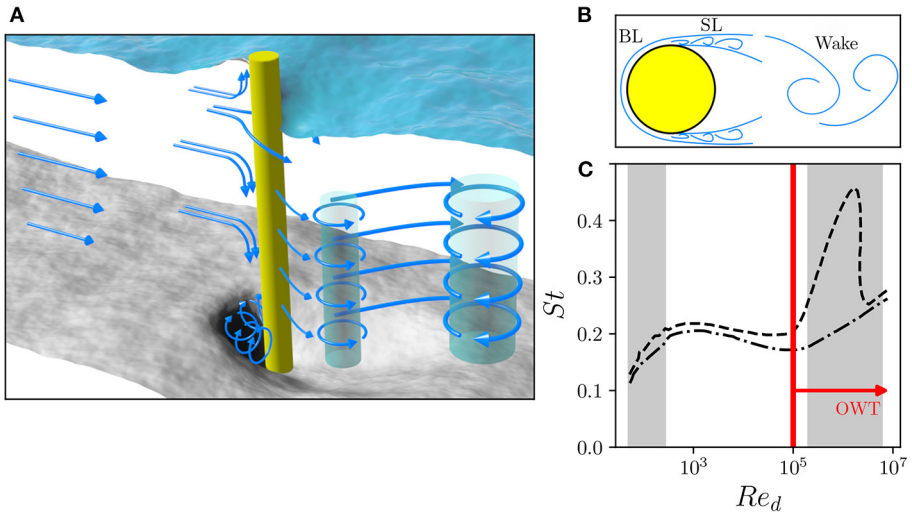

FIGURE 8 | Typical flow past a cylinder. **(A)** Shows the finite-depth 3D flow past a cylinder over an erodible bed, depicting the shedding Karman vortices (KV). Note, although not discussed herein, the run-up/depression at the water surface upstream/downstream of the cylinder and formation of horseshoe vortices cause scour at the bed, which may destabilize structures (Matutano et al., 2013). **(B)** Shows the three shear layers comprising the cylinder flow: BL denotes the boundary layer and SL denotes the shear layer. **(C)** Shows the typical $Re_d - St$ relationship for flow past a cylinder. Shaded regions represent the 2D laminar vortex shedding regime ($49 \lesssim Re_d \lesssim 192$) and the trans-critical flow regime ($2 \times 10^5 \lesssim Re_d \lesssim 6 \times 10^6$). Upper curve represents flow for a smooth cylinder, lower curve for a rough cylinder. Curves are based upon the experiments reviewed by Lienhard et al. (1966). The red line indicates the expected minimum Reynolds number of an OWT.

studies are directly analogous to flow past OWT foundations, such as monopiles. Unsteady vortices shed by cylinders can lead to vibration, acoustic noise, resonance, and ultimately structural failure. Shed vortices form coherent wakes that are spatially vast, and can be detected several hundred diameters downstream of their source, depending on the background flow conditions (e.g., turbulence properties). Cylinder wakes fundamentally alter flow conditions as a source of anthropogenic turbulence (mixing), particularly coherent along the cylinder axis. Dynamics are complex due to the interaction of at least three shear layers; the boundary layer, shear layer, and wake (**Figure 8**). In unstratified waters, flow structure is dependent on the cylinder roughness, end conditions, freestream conditions, and the ratio of inertial to viscous forces, the cylinder Reynolds number Re_d,

$$Re_d = \frac{u_\infty d}{\nu}, \tag{8}$$

where u_∞ denotes the freestream velocity, d the cylinder diameter and ν the fluid viscosity. The dependence of the flow structure on Re_d arises due to transitions in the different shear layers. The most well known instability arising from the flow past a cylinder is the Karman vortex (KV) (Williamson, 1996), which develops for $Re_d \gtrsim 49$ (below which the flow is steady and laminar). The Karman instability is associated with alternating 2D vortices shed from either side of the cylinder, aligned with the cylinder axis, and is a consistent feature of even high Reynolds number flows. The unsteady KV is characterized by the dimensionless frequency, the Strouhal number $St = f_{KV} d/u_\infty$, where f_{KV} is the frequency of vortex shedding. St varies with Re_d depending on shear layer transitions, as shown in **Figure 8C**. The KV is a dominant feature of flow past a cylinder (**Figure 9A**).

The typical Re_d of shelf sea currents past offshore wind foundations (**Figure 2**) is at least $Re_d \gtrsim 10^5$, estimated assuming a small 5 m diameter monopile with a minimum tidal velocity of 0.02 m s^{-1} (Vindenes et al., 2018). This minimum Reynolds number is sub-critical (see **Figure 8**), indicating that shear layer instabilities may be present, manifesting as Kelvin-Helmholtz (KH) type instabilities. Three dimensionality is a dominant feature of cylinder wakes at these high Reynolds numbers. Critical transition occurs between $2 \times 10^5 < Re_d < 5 \times 10^5$, and is associated with boundary layer transition to turbulence which causes the separation point to occur further downstream on the cylinder surface. For a smooth cylinder, asymmetric separation-reattachment of the boundary layer either side of the cylinder causes a sudden increase in vortex shedding frequency (**Figure 8**). Super-critical flow is associated with $Re_d > 5 \times 10^5$, where symmetric separation bubbles and turbulent boundary layers are present on both sides of the cylinder. Roughness effects are felt primarily in the critical transition regime; surface roughness causes earlier transition to turbulence and bypasses the asymmetric regime (**Figure 8B**).

With distance x downstream, the far-wake $x/d \gtrsim 50$ is particularly sensitive to freestream conditions. The spectral energy of the KV (energy associated with f_{KV}) decays downstream of the cylinder and the wake width grows like $\sqrt{x}$ (under low levels of freestream turbulence) and is approximately self-similar (Ghosal and Rogers, 1997). A secondary vortex street emerges at a lower frequency than the KV, arising due to the merging of vortex pairs, or via hydrodynamic instability of the mean flow, depending on the flow Reynolds number (Jiang, 2021a). Coherent structures in the far-wake can also arise due to non-linear interactions between freestream structures

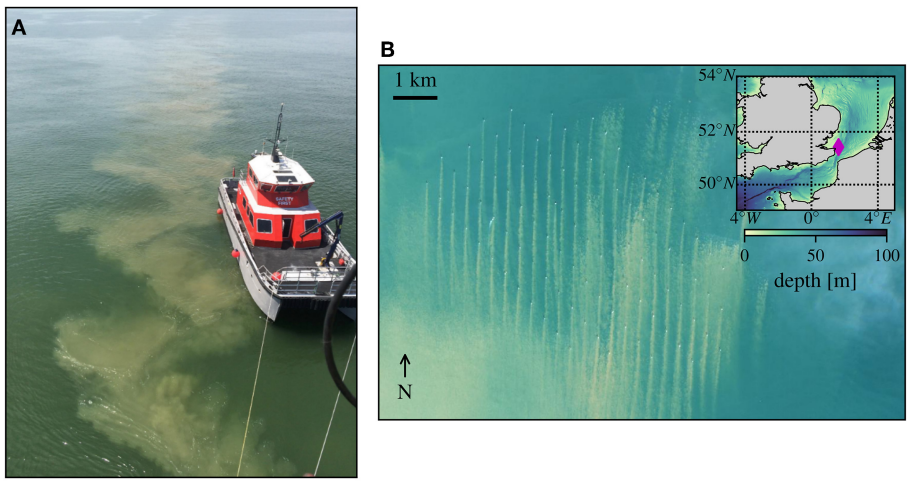

FIGURE 9 | Sediment plumes generated by cylindrical structures. **(A)** Wake and turbid plume showing the coherent Karman street from the lee of a metocean mast, image courtesy D. van der Zande. **(B)** Satellite imaging of turbid plumes show they extend over multiple kilometers, individual monopile diameters are $d = 4.3$ m, image courtesy R. Forster (Forster, 2018). With average monopile spacing of 1 km, interactions of the turbid plumes are clearly visible.

and the KV. Cimbala and Krein (1990) and Williamson and Prasad (1993) found that the interaction between the KV and freestream waves could lead to resonant peaks in spectral energy associated to their non-linear interaction, indicative of hydrodynamic instability. These peaks can be detected far downstream of the cylinder, $x/d > 300$, indicating that non-linear dynamics have a large effect on the wake even far downstream. It is therefore unsurprising to observe non-linear interaction between wake effects from multiple monopiles in offshore wind farms (**Figure 9**). Under high freestream turbulence the wake spreads more rapidly, depending on the background turbulent intensity and the turbulent integral length scale. Eames et al. (2011) demonstrated that the growth rate of the wake increases from $\sim \sqrt{x}$ to $\sim x$ when the wake deficit velocity is approximately equal to the background turbulent intensity, and the integral length scale of the turbulence is comparable to the cylinder diameter. When subject to high turbulence a cylinder wake will dissipate downstream more rapidly and diffuse into the background turbulence. In contrast, when background turbulence levels are low the turbulence generated in the wake of a cylinder can persist hundreds of diameters downstream.

In current shallow-water offshore wind farms, where levels of turbulence are high, wakes have been observed at least 1 km in length (e.g., **Figure 9**). The formation of turbid plumes, where suspended sediment is trapped and transported in KVs and secondary vortex streets, is correlated with high levels of TKE (Grashorn and Stanev, 2016). As the wakes pass through the wind farm plumes are observed to spread and interact (**Figure 9B**). Wake spreading indicates that the effects of monopile wakes are not limited to a short narrow region downstream. Although KV are expected to decay for $x/d \approx 60$ (Jiang and Cheng, 2019), observed plume interaction at large lengths, $x/d > 150$, suggests wake-wake interactions are important. However, conditions vary considerably between the current shallow coastal offshore wind farms and the deep water future development sites. It is to be expected that in deep water sites, with lower background turbulence, that wakes may be even larger.

3.2. Stratified Flow

Relatively few studies have investigated stratified flow interaction with vertically oriented cylinders, analogous to proposed offshore wind foundation deployment in seasonally-stratified shelf seas. This may be in part due to similarity between unstratified and stratified flow past vertical cylinders at very low Reynolds, $Re_d \lesssim 45$ (Meunier, 2012), where wakes are inherently two-dimensional. However, differences arise when three-dimensionality is present in the wake, which is certainly characteristic of the high Reynolds number flows associated with offshore wind farm infrastructure. Three-dimensionality in the wake of vertical cylinders is important as it can lead to fundamental reorganization of stratified fluids. Layering can emerge where such a flow can lead to multiple intermittent regions of fairly constant density neighboring thin interfaces with steep density gradients (Bosco and Meunier, 2014). This layering behavior may arise from any process that produces spatially periodic mixing in the vertical direction (Thorpe, 2016).

Cylinder wakes are prone to layering due to their increase in both horizontal shear, normal to the direction of stratification, and organized vertical vorticity, parallel to the direction of stratification, through the formation of KV in particular. The susceptibility of a stratified flow, perturbed by moving cylinders, to layering is dependent on the mechanisms that generate layers, which vary considerably depending on the type of forcing (e.g., oscillatory vs. continuous stirring, Thorpe, 2016). Experiments have demonstrated that layers can develop from the 'cloud' of stratified turbulence that results from dragging vertical cylinders through a stratified flow, equivalent to flow through a wind farm (**Figure 10**). In the experiments of Maffioli et al. (2014)

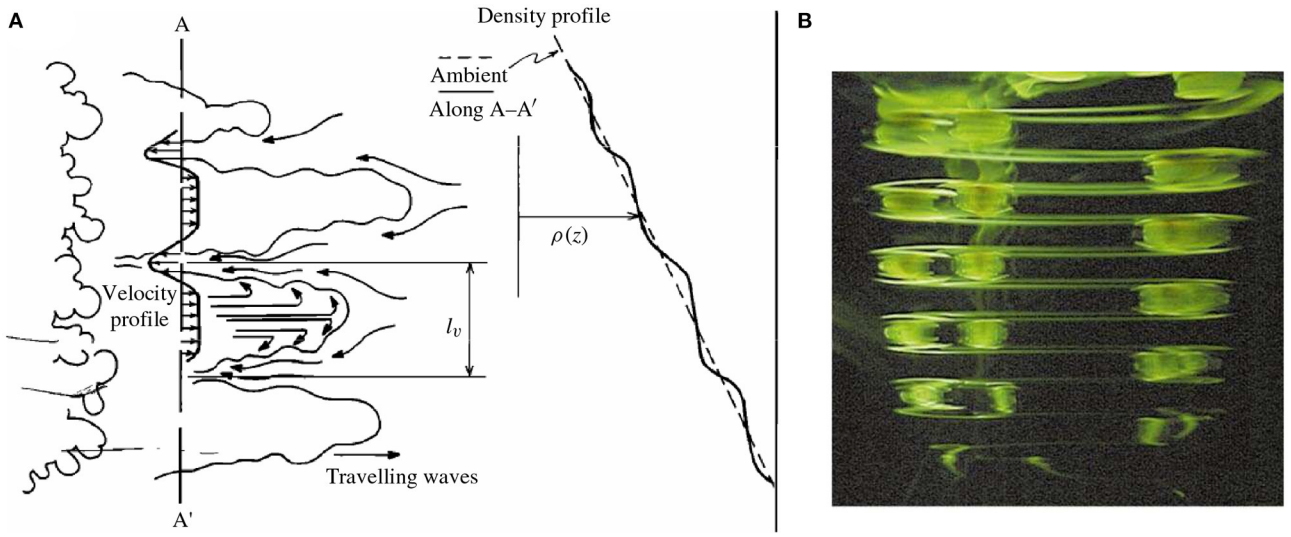

FIGURE 10 | Layering in a linearly stratified fluid emerging from a turbulent cloud, with the resulting density profile across the intrusions **(A)**, from Maffioli et al. (2014). A Dye visualization of the zig-zag instability is presented in **(B)**, from the experiments of Billant and Chomaz (2000a).

intrusions developed from local regions of mixed fluid, which grew until their length scales were approximately balanced by $l \sim \tilde{u}/N$, where $\tilde{u}$ represents a characteristic velocity scale of the turbulence. The buoyancy frequency may also be used to define a Froude number, the ratio of inertial to gravitational forcing, where L is some length scale over which flow velocity and N are averaged,

$$Fr = \frac{\tilde{u}}{NL}. \tag{9}$$

Thus, in the experiments of Maffioli et al. (2014), packets of turbulent fluid grew until they collapsed under gravity ($Fr \sim 1$) and spread outwards as pancakes, triggering horizontally propagating internal waves. The outward spread of intrusions generates a layered density profile, where well-mixed intrusions are neighboured by thin regions of strong density gradient. It is important to note here that the cylinders are not critical to the reorganization of stratification; they only act as the source of turbulence, via horizontal shear, in the stratified flow. Addition of purely horizontal shear to simulations of stratified shear flow can lead to coherent vertical vortices (Basak and Sarkar, 2006), analogous to the KV and KH instabilities of a cylinder wake. The coherent vertical vortices exhibit pairing, tearing, and amalgamation, resulting in a complex braided vorticity structure that ultimately leads to vertical variability. Layers can subsequently develop as intrusions, coupled with internal waves (Basak and Sarkar, 2006), once again with a characteristic vertical scale of the order of $\tilde{u}/N$, when these two quantities are estimated appropriately.

Indeed, provided the flow Reynolds number is sufficiently large, there is accumulating evidence, that horizontal shear (and hence vertical vorticity) in vertically stratified fluids inevitably forms layers on this scale. Dating back to the first theoretical analysis of Billant and Chomaz (2000b), there is clear evidence that such flows are prone to a class of 'zig-zag' instabilities. These instabilities imprint the $\tilde{u}/N$ vertical scale on the flow, and can be connected directly to the inherently nonlinear layered structures that develop at finite amplitude (Lucas et al., 2017). Furthermore, several studies (Deloncle et al., 2008; Waite and Smolarkiewicz, 2008; Augier et al., 2015) have demonstrated that the breakdown of these vertical vortices in a stratified fluid introduce a new, inherently stratified route to turbulence in a stratified fluid, and hence substantially enhanced mixing.

Whilst work on layering has been restricted to small scale experiments and comparatively low Reynolds numbers (at least by oceanographic standards), it has provided oceanographers with vital information on the fine-scale density structure of the ocean. However, it is unclear how turbulence generated at high Reynolds number, by flows past offshore wind foundations, will interact with the essentially two-layer density profile of seasonally stratified shelf seas. In addition to the high Reynolds number, offshore wind foundations are a similar width to the typical thermocline thickness. This contrasts with previous work where turbulence was either generated by structures with length scales two orders of magnitude smaller than the density gradient length scale (Maffioli et al., 2014), or (as in the 'zig-zag' instability studies mentioned above) the unstable horizontal shear/vertical vorticity is embedded initially in a linearly stratified fluid with close to constant buoyancy frequency. Where KV shed from offshore wind foundations are of the same order diameter as the density gradient length scale, flow mixing and density profile reorganization may be fundamentally different, and this generic stratified flow geometry with a range of key characteristic length scales is very poorly understood, even in highly idealized circumstances.

Expansion of the offshore wind sector to deeper waters is predicated on development of floating foundations, which are finite in depth and anchored to the seabed. Finite depth structures

induce complex dynamics within stratified fluids, especially if structures intersect sharp density gradients, i.e., the thermocline (**Figure 2**). A good example case study of the impact of finite depth obstacles on stratified flow, is flow past a horizontal cylinder. At high Froude numbers dynamics are similar to unstratified flow. But as the Froude number decreases several new regimes occur (Boyer et al., 1989). Under stratification internal waves can be generated not only by the structure but also the KV. This in turn can increase drag, and thus the amount of mixing, by up to 100% (Arntsen, 1996). The drag coefficient of spheres in stratified flows also varies by up to 100%, when the vortex shedding frequency tends to the buoyancy frequency (Cocetta et al., 2021). A variety of fixed and floating foundations may be susceptible to such additional drag, where vortices shed are not necessarily aligned with the direction of stratification (e.g., jackets and semi-submersible foundations, **Figure 2**).

Through considering reflectional symmetry, flow past floating foundations may be analogous to oceanic and atmospheric flow past sea-mounts and hills. Stratified flow past such obstacles displaces fluid and leads to both vertically and horizontally propagating internal waves, as well as a significant downstream wake (**Figure 11**).

If an obstacle is wide compared to its height, most fluid impinging on the obstacle passes over it, otherwise flow can pass around it. For low Froude numbers, where L is scaled with obstacle depth, flow blockage by internal waves creates additional drag, which is a very effective momentum sink on the impinging flow. Flow blockage can increase the drag force by 1–2 orders of magnitude compared to unstratified flow over the same obstacle (Smith, 1978; Castro et al., 1990; Cummins et al., 1994). In all cases understanding drag increase is critical to evaluate both the hydrodynamic loads placed on foundations and anchors, and the mixing in stratified shelf seas, associated with the flow past offshore wind foundations. Such wave generation and propagation also suggests the possibility that the effect of flow structures can be both local and non-local, as the emitted waves may transport momentum flux significant distances until they 'break'.

3.3. Mixing of Stratified Shelf Seas by Offshore Wind Foundations

To date there has been only two limited studies observing offshore wind foundation induced mixing of stratified waters (Floeter et al., 2017; Schultze et al., 2020a). These studies have been restricted to developments in aperiodically stratified regions of freshwater influence, in shallow water (depths of approximately 40 and 24 m, respectively). Neither studies have investigated the potential impacts on seasonally, or permanently, stratified shelf seas.

Floeter et al. (2017) performed surveys on two wind farms in the German Bight, North Sea. Water property transects through the wind farm revealed a consistent weakening of stratification near the centre. Effects extended into the surrounding area by approximately half the diameter of an ambient tidal excursion. However, it was unclear how much of this was due to 'infrastructure' turbulence from turbine foundations rather than natural topological effects. In addition to reduced stratification, Floeter et al. (2017) also measured local upwelling at the edges of the wind farms, similar to those observed near islands in stratified waters (e.g., Simpson et al., 1982). Shallow water model studies of the effects of offshore wind farms on local oceanic circulation patterns have shown arrays of infrastructure induce strong horizontal shear in wind stress leading to local regions of upwelling and downwelling (Broström, 2008; Paskyabi and Fer, 2012), consistent with the observations of Floeter et al. (2017).

Field measurements were also taken by Schultze et al. (2020a) who measured the stratified wake from an offshore monopile at the leading edge, with respect to local flow, of the DanTysk wind farm (**Figure 12**). The monopile wake spread to a width 10 times the (6 m) diameter of the monopile and had reduced the potential energy anomaly by up to 65 % at a downstream distance of $x/d \approx 20$ (**Figure 12**). The full distance required to return to pre-monopile conditions was not captured by the survey, even after approximately 300 m, a distance over 50 times the 6 m monopile diameter. The survey clearly demonstrates that turbulence generated by monopiles reduces stratification. Complementing the survey, Schultze et al. (2020a) used Large Eddy Simulations (LES) to model flow past a single monopile which was simulated under different levels of background stratification. TKE dissipation rate was found to be up to two orders of magnitude larger in the thermocline than when monopiles were not present. High TKE dissipation rate persisted far downstream of the cylinder and, at $x/d > 40$, was still an order of magnitude larger than without monopiles at the thermocline depth. Further, the TKE dissipation rate was greater than that generated by the bottom boundary layer.

During a period of stronger stratification, Schultze et al. (2020a) conducted a second survey at the opposite end of the DanTysk wind farm. The second survey was less conclusive than their previous measurements, finding that no clear signal from the wake could be separated from background variability. This may be because stratification was strong enough to suppress the growth and interactions of the wakes, although (Schultze et al., 2020a) only sampled the wake at distances greater than 200 m (or 33.3 diameters) from the monopile. It is therefore unclear if this is a result consistent with the earlier survey in **Figure 12**.

Leading order arguments for the mixing induced by offshore wind foundations have been explored by Rennau et al. (2012) and Carpenter et al. (2016), here they are reviewed. Models start by assuming that the turbulence produced by foundations is equal to the power lost to drag. Over an arbitrary vertical layer of fluid, L, the power lost to drag is given by

$$P_D = \frac{1}{2}\rho c_D d L \langle |\mathbf{u}|^3 \rangle_L, \tag{10}$$

where c_D denotes a drag coefficient and $\langle |\mathbf{u}|^3 \rangle_L$ the velocity magnitude cubed, averaged over the layer L. Whilst, Rennau et al. (2012) and Carpenter et al. (2016) assumed that c_D is a constant in reality it is variable and dependent on the Reynolds number, surface roughness and structure geometry. The drag coefficient is also likely a function of depth and time and will vary with

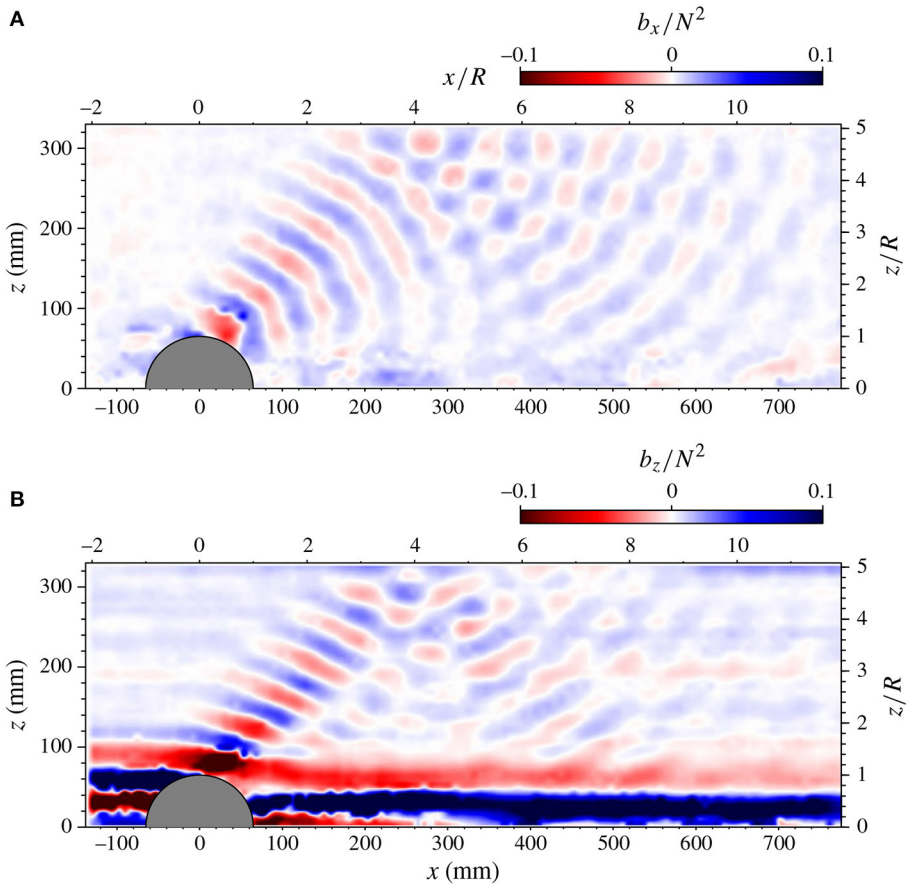

FIGURE 11 | Stratified flow over a hill, taken from the experiments of Dalziel et al. (2011). Internal waves can be observed in the lee of the structure propagating vertically and horizontally, clear in both **(A)** the horizontal buoyancy gradient $b_x = -\partial\rho/\partial x$ and **(B)** vertical buoyancy gradient $b_z = -\partial\rho/\partial z$. The wake is also particularly apparent in the b_z field, demonstrating the existence of significant mixing. N is the background buoyancy frequency and R denotes the height of the hill.

background shear. Crucially c_D is also dependent on the Froude number, especially for highly stratified flows (see Section 3.2). At present there is no parametrisation of the Froude number dependence of the drag coefficient for vertical infrastructure in stratified flows. We therefore assume $c_D = 1$ as per the "high drag" case of Carpenter et al. (2016), although this estimate does not account for the potential effects of the Froude number.

A wind farm comprises many turbines, potentially supported by a range of foundations. Turbines are separated by a distance of approximately $10D$ (Howland et al., 2019), where D is the rotor diameter. The average production of TKE per unit volume $\mathcal{P}_D$ over a layer of thickness L is therefore:

$$\mathcal{P}_D = \frac{1}{2}\frac{\rho_0 c_D d\langle|\mathbf{u}|^3\rangle_L}{100D^2}. \tag{11}$$

Here it is assumed that the power lost to drag at a turbine foundation acts to increase TKE production over the full area occupied by a foundation. In reality this production will be localized to the comparatively narrow wake, and will vary by several orders of magnitude in space.

Here the potential production of TKE $\mathcal{P}_D$ per unit volume, generated by the addition of a 10 m diameter monopile, is estimated using the natural conditions, averaged over the thermocline thickness, at the CaNDYFLOSS experiment site (**Figure 3**). Power generated by flow past such a potential foundation is strongly dependent on the flow velocity, with low frequency oscillations associated with neap-spring tide cycles and higher frequencies associated to daily tidal cycles (**Figure 13**). The potential power added to the thermocline, $\mathcal{P}_D$, varies between approximately $2 \times 10^{-6}\,\mathrm{W\,m^{-3}}$ to $4 \times 10^{-4}\,\mathrm{W\,m^{-3}}$ with an average value of $5.9 \times 10^{-5}\,\mathrm{W\,m^{-3}}$. Over the same period, at the same site, the natural background dissipation rate (ε_B) at the thermocline is $3.5 \times 10^{-5}\,\mathrm{W\,m^{-3}}$ (Scannell et al., 2021). In this approximate calculation, the additional (average) turbulence production is therefore 69% greater than background dissipation without monopiles present: $\mathcal{P}_D \approx 1.69\,\varepsilon_B$.

Under several very strong assumptions, the relation between TKE produced by offshore wind foundations and how it is balanced by viscous dissipation and work performed on the

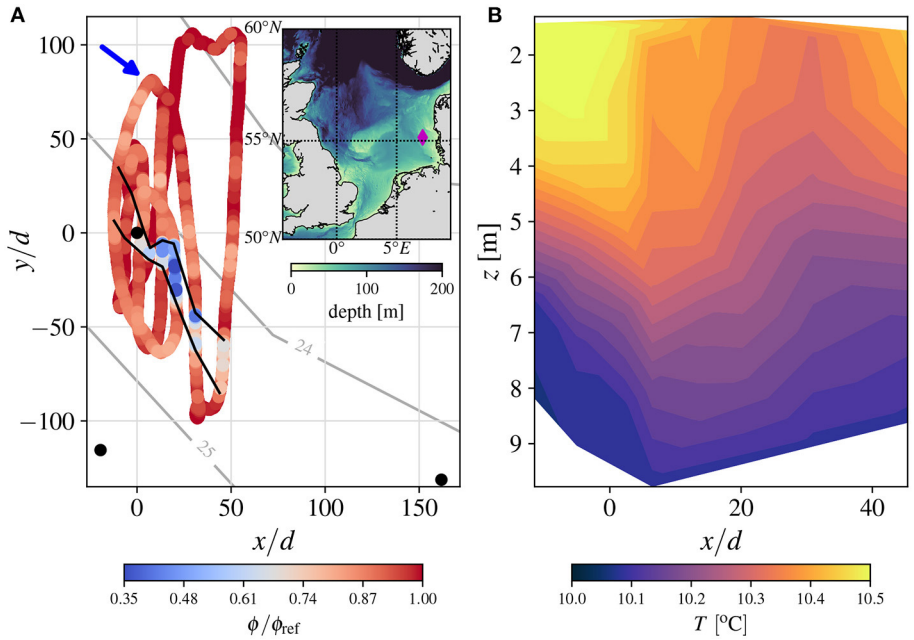

FIGURE 12 | Observations of the turbulent stratified wake downstream of a monopile, derived from the survey conducted by Schultze et al. (2020a). The monopile of diameter 6 m, is located at 55.16°N 7.07°E on the leading edge, relative to local flow, of the DanTysk wind farm. The wind farm is marked by the diamond in the inset figure of **(A)**. **(A)** Depicts the potential energy anomaly, ϕ around the monopile. ϕ is normalized by its background reference value, ϕ_{ref}. The approximate flow direction is indicated by the blue arrow, and neighboring monopiles are marked by black circles. The wake is clearly visible by the blue regions, and approximately enclosed by the black lines. **(B)** Shows the spatial development of the temperature field in the flow before and the wake after the monopile. Evolution of the temperature field is obtained by averaging data in the regions enclosed by the black lines in **(A)**. Data are from Schultze et al. (2020b).

buoyancy field may be expressed, from Equation (3), by

$$\mathcal{P} = \mathcal{P}_D + \mathcal{P}_B = (1+\Gamma)\varepsilon_D + (1+\Gamma)\varepsilon_B, \tag{12}$$

where subscript D represents contributions from structures (drag) and subscript B represents all other (background) contributions to TKE production ($\mathcal{P}$) and dissipation rate (ε).

For simplicity, the turbulent flux coefficient can be assumed equal for each component of B and ε such that $\Gamma = B/\varepsilon = B_B/\varepsilon_B = B_D/\varepsilon_D$. In deriving (12) it is also assumed that OWT infrastructure contributes linearly to $\mathcal{P}$, and is simply related to the structure-induced TKE dissipation rate by $\mathcal{P}_D = (1+\Gamma)\varepsilon_D$. In the present example we have shown that $\mathcal{P}_D \approx 1.69\varepsilon_B$, such that

$$\mathcal{P}_D = (1+\Gamma)\varepsilon_D \approx 1.69\varepsilon_B. \tag{13}$$

Under the simplest conventional assumption that $\Gamma = 0.2$, as typical at the pycnocline in seasonally stratified waters (see Section 2), we obtain $\varepsilon_D \approx 1.4\varepsilon_B$, such that the total TKE dissipation rate, $\varepsilon = \varepsilon_B + \varepsilon_D$, is at least 140 % higher at the thermocline when OWT infrastructure is present. As noted, several sweeping assumptions have been made to arrive at this estimate, which inevitably has a large amount of implicit uncertainty. It is reasonable to suppose that this estimate is likely to be a conservative lower bound on the effect of OWT infrastructure on turbulent dissipation and mixing at the thermocline for at least two reasons. The first is that there is clear potential for a strongly nonlinear effect of such infrastructure on the dissipation rate. Secondly, setting $\Gamma \simeq 0.2$ may well be an under-estimate of the vigorous overturning mixing likely to be triggered in the wake of such infrastructure (Caulfield, 2021). Nevertheless, these simple conservative estimates show that foundations produce turbulence at levels that will clearly affect the leading order balance of TKE transport, even when normalized by the *total* area between offshore wind foundations. Thus, offshore wind has the potential to impact directly the stability of seasonally-stratified shelf seas (**Figure 5**).

The dissipation rate estimate indicates that OWT infrastructure is likely to affect the leading order balance of TKE transport in vicinity of the windfarm, but the implications of this on regional-scale fluid dynamics is more challenging to evaluate. To address this, Carpenter et al. (2016) derived similar models for TKE production as Equation (11), and constructed arguments based on estimates of the different timescales in the flow. In particular, timescales of OWT-induced mixing, and timescales of flow parcels convecting through the windfarm. By comparing different estimates of these timescales Carpenter et al. (2016) theorised the extent that the water column would mix as a parcel passed through the array. It was concluded that small developments in shallow waters (Bard 1 and Global Tech 1, German Bight) were unlikely to affect stratification, where TKE production from the bed and free surface dominate. However, despite the simplification of the models and assumptions made, large scale developments in deep water were recognized to have potential for significant impact (Carpenter et al., 2016).

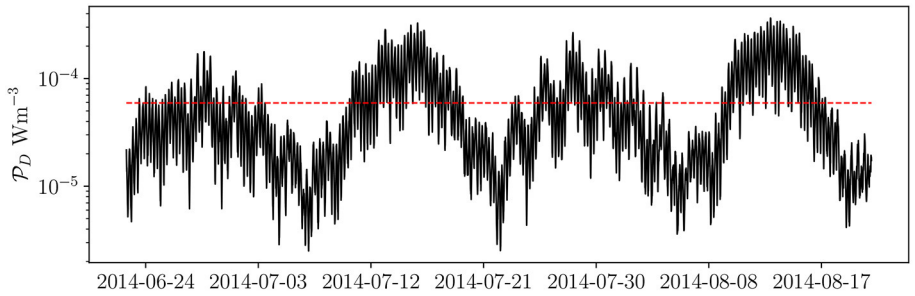

FIGURE 13 | Mean TKE production by a $d = 10$ m offshore monopile. TKE production is based on direct velocity measurements averaged over the thermocline, 20–50 m in the Celtic Sea between 22/06/2014 and 20/08/2014, **Figure 3** (Scannell et al., 2021). Turbulence production (Equation 11) is closed by assuming $c_D = 1$, $\rho_0 = 1.000\,\mathrm{kgm}^{-3}$ and $D = 200\,\mathrm{m}$. The power averaged over the full time period is marked in red.

Rennau et al. (2012) adopted regional-scale numerical models to assess the effects of offshore wind development in the Baltic Sea, where tidal currents are minimal and stratification are driven by dense saline currents beneath fresher water. They modified a two-equation (RANS) turbulence closure scheme to capture the enhanced mixing arising from OWT installations and found that current installations did not have a significant effect on regional stratification (though cautioned that future development, covering more of the Western Baltic Sea, could lead to significant impacts, such as reduced bottom salinity). However, these closure schemes are known to be overly dissipative in stratified flows (Hewitt et al., 2005), and demonstrated to generate overly diffuse pycnocline structures in realistic simulations (Luneva et al., 2019). These schemes are therefore improperly conditioned, at present, to address the impact of OWT infrastructure in stratified seas.

Cazenave et al. (2016) adopted a similar oceanographic model to Rennau et al. (2012) and attempted to explicitly resolve the structure-induced wakes shed from wind turbines using local grid refinement. They modeled the effects of windfarms in the essentially well mixed (unstratified) Irish Sea, where dissipation rates in the water column are already high (Simpson et al., 1996). However, they did not modify the closure scheme to account for wake generated turbulence. Whilst visualizations of turbine wakes by Cazenave et al. (2016) are in qualitative agreement with sediment plumes observations (**Figure 9**), accurate prediction of wake associated mixing in stratified waters still require advances in fundamental physical process understanding to enable development of appropriate turbulence closure schemes (Rennau et al., 2012).

4. DISCUSSION

The scale of planned offshore wind energy industry is much greater than past, and existing, sea use. Installed offshore wind capacity will increase by 600% in the next decade (**Figure 1A**), requiring an extra $\sim$ 20,000 10 MW+ turbines. Fixed, and floating, offshore wind infrastructure will penetrate the thermocline, adding 'anthropogenic' mixing on top of natural mixing. The impact of such infrastructure will be fundamentally different from existing sea use. For example, even large surface vessels have comparatively small drafts, $\sim$10 m (Golbraikh and Beegle-Krause, 2020; Nylund et al., 2020). Further, whilst offshore oil and gas platforms are similar to offshore wind infrastructure, spanning the thermocline, only $\sim$ 6,500 platforms have been installed, globally, over the last 75 years (Schneider and Senders, 2010). Therefore, planned offshore wind developments will add new and large scale infrastructure sources of turbulent mixing in seasonally stratified seas. This discussion reviews our current knowledge gaps, frames potential impacts on shelf sea dynamics and thus marine ecosystem functioning and highlights routes for sustainable growth of the offshore wind sector.

4.1. Infrastructure Mixing

The mixing of stratified waters by offshore wind infrastructure is poorly understood. As evidenced in Section 3.3 there is a dearth of research on high Reynolds number stratified flow past vertical structures, which is vital for understanding and parameterizing 'infrastructure' mixing processes in natural environments. The problem is particularly complex due to its scale; laboratory experiments and fully resolved numerical simulations are limited to relatively low Reynolds number flows, certainly by comparison to the real oceanographic flows. In all scenarios of fixed or floating OWTs, fine scale vertical density structure and enhanced mixing is anticipated due to horizontal shear generated by the flow past the infrastructure. The $\mathcal{O}\left(10^{-2} - 10^{0}\right)$ m length scales associated with the resulting turbulence will be unresolved by low resolution numerical simulations. Wakes from individual structures may persist for $\mathcal{O}\left(10^{2} - 10^{3}\right)$ m downstream. From individual wind turbines to a single offshore wind farm, infrastructure adds a wide range of length scales of $\mathcal{O}\left(10^{1} - 10^{4}\right)$ m. Further, multiple wind farms are distributed at shelf-wide scales. The vast range of length scales present in flow past offshore wind farms necessitates a variety of modeling techniques.

Coarse numerics, i.e., Large Eddy Simulation (LES) or other more sweeping turbulence closure schemes, may be desirable modeling strategies for high Reynolds number flow (Rennau et al., 2012; Carpenter et al., 2016). Nested or adaptive meshing, in particular around known boundaries such as OWT foundations (see, e.g., Rennau et al., 2012; Cazenave et al., 2016), can be used to further reduce numerical cost or improve simulation accuracy.

However, without a firm understanding of the underlying physics, e.g., from fully-resolved simulations, or robust datasets for validation, low resolution numerical models should be adopted with care, particularly for stratified (and therefore highly anisotropic) flows (Hewitt et al., 2005; Khani and Waite, 2015). Integration of modeling disciplines ranging from Direct Numerical Simulation (DNS) of idealized flows to regional scale, operational forecast, ocean circulation models is therefore required to determine the impact of offshore wind farms, which scale to natural features and processes inherent to seasonally stratified shelf seas (**Figures 1**, **4**, **6**). Field surveys are essential to support and validate physical and numerical studies. However, the limited work to date (Floeter et al., 2017; Schultze et al., 2020a) has suffered from uncertainties, where either effects of infrastructure were difficult to discern from topographical effects or where wakes were difficult to separate from background variability. While both studies concluded effects of infrastructure on mixing may be large, further surveys are required to support this. In addition there is a clear need for repeat and 'before and after' surveys, as noted by van Berkel et al. (2020).

There are also key research questions regarding the geometry of offshore wind infrastructure, and how this impacts mixing. OWTs shed vortices with horizontal scales that are comparable to the thickness of the thermocline. Such mixing contrasts with previous work studying mixing by thin vertical cylinders, several orders of magnitude smaller in diameter compared to density length scales. It is vital to understand how large scale vortex structures interact with a relatively thin thermocline; they could produce Langmuir-like interactions with the thermocline (Polton et al., 2008), or mixing processes may well be fundamentally different to those studied before, with complex spatio-temporally variable vortex, turbulence and mixing dynamics. In addition, future floating technology raises further questions regarding the impact of geometry on mixing. It is expected that spar-buoy designs (**Figure 2**) will act in a similar way to monopiles, given they penetrate through the thermocline and into the well-mixed deep water. However, semi-submersible (or any other small-draft designs) will introduce non-trivial effects by intersecting the thermocline. Research of stratified flow over finite topography, similar to small draft floating OWT, has demonstrated that baroclinic effects can enhance drag by up to two orders of magnitude (Section 3.2). Here, floating structures will introduce infrastructure mixing via shed lee waves, internal waves, blockage effects, and wake-wake interactions in the case of semi-submersible designs.

Crucially, a lack of insight into key multi-scale mixing processes adds uncertainty to current attempts to quantify the impact of infrastructure mixing on shelf sea dynamics and ecosystem functioning. For example, the turbulent flux coefficient is often assumed constant, $\Gamma = 0.2$ (Section 2.3 and 3.3), but it is unknown if this holds in the wake of OWTs where fine scale density structures and strong spatial variability are present. Further, production of TKE due to infrastructure has been assumed constant in time and evenly distributed over the area 'occupied' by the monopile. In reality production is focused in the narrow wake of individual monopiles, and could vary by two orders of magnitude during the spring-neap tidal cycle (Section 3.3). TKE production, and thus mixing, arising from stratified flow past infrastructure is also dependent on the drag coefficient c_D, yet little is known about the dependence of c_D, particularly at high Reynolds numbers or where mixing length scales are large in comparison to density length scales. Meanwhile, research on drag past other obstacle forms suggest estimates for drag may be incorrect by orders of magnitude. Advancing our understanding of each of these processes is vital for assessing their impact on shelf sea oceanography and ecosystem functioning.

4.2. Shelf Sea Dynamics

Offshore wind farms are anticipated to have large local impacts on shelf sea dynamics, in a similar fashion to natural topographically controlled mixing, e.g., driven by internal waves and flow over seafloor sand banks. It is anticipated that a broad and more diffuse thermocline would develop as a result of enhanced mixing, weakening it as a barrier to vertical mixing and transport (**Figure 14**). Subsequent change to surface water characteristics would likely alter exchange across the ocean-atmosphere interface, with impacts on heat storage, atmospheric CO_2 uptake and benthic resupply of O_2. The scale of this response will be site and infrastructure specific. At regional scales the water column should re-stratify subject to natural buoyancy forcing. In a more extreme scenario, strongly enhanced mixing could prevent stratification from forming around wind farms. This effect is observed around islands, where reduced surface temperatures and well-mixed waters result from enhanced mixing due to flow acceleration and seabed shoaling (Simpson et al., 1982). Small, but significant residual currents sweep this well-mixed water into an observable downstream wake.

Enhanced mixing from infrastructure may also impact seasonal, and shorter timescale, cycles. The first order response of the vertical density structure to enhanced mixing in a wind farm region would likely be delayed onset and early breakdown of seasonal stratification with weaker stratification throughout the summer season. Development of near surface stratification during periods of low wind stress would no longer be expected to occur as the enhanced mixing would act to persistently stir the normally episodically mixed surface layer.

With infrastructure development from local scale of a single turbine to regional scales of multiple developments offshore wind farms in shelf seas have the potential to have regional impact. Horizontal variation in density may arise from wind farm scale mixing, and these variations may enhance submesoscale processes driving additional vertical transport and mixing. Advanced regional oceanographic models, which integrate physics based closures of offshore wind farm driven mixing, will be required to understand impacts of such large scale processes. The density of offshore wind farms and the regional distribution of mixing and wake-wake interactions between wind farms will be of critical importance in determining shelf sea response to offshore wind development.

As has been discussed herein, deployment of OWT foundations will lead to significant enhancement of natural sub surface shear-production of turbulence, mixing the thermocline. However, OWT also generate significant atmospheric wakes,

which can extend downstream over multiple array scales, and upstream wind blocking effects (Howland et al., 2019; Nygaard et al., 2020). Changes in atmospheric wind speed or location of stably stratified atmospheric boundary layers, due to atmospheric wakes and wind blocking, will impact air-sea exchange of heat, momentum and trace gases. Sea surface wind shear mediates the rates of air-sea exchange of momentum, heat and trace gases, e.g., CO_2 (Komori et al., 1993; Lincoln et al., 2016). Wind speeds are further directly coupled to surface wave dynamics. Change in wind speeds, decreasing turbulence production by wave breaking, would result in changes to wave-driven Langmuir turbulence which may extend across the near surface well mixed layer (see, e.g., Lucas et al., 2019). Indeed the interaction between the Stokes shear and the vertical vortices shed from the infrastructure might energize the Langmuir turbulence to establish a modified equilibrium mixed layer depth (Pearson et al., 2015). In consequence the complex interplay of oceanic surface mixed layer and atmospheric dynamics arising from development of OWT in stratified shelf-seas will be a key area for future research.

4.3. Shelf-Sea Ecosystem Functioning

Enhanced mixing rates due to infrastructure, would not only lead to temporal and spatial variations in vertical density structure, but also impact biogeochemical function at a fundamental level that would cascade up the ecosystem.

Stronger mixing in the thermocline will drive more nutrients from the bottom water up into the subsurface chlorophyll maximum and, if the mixing is strong enough, up into the surface layer where it could support additional phytoplankton growth. The rate of turbulent mixing strongly affects the simulation of ecosystem behavior, as demonstrated by Luneva et al. (2019), who found that different mixing schemes caused a shift in the spring bloom by 1 month, and change regional chlorophyll differences by order 100%.

Mixing also alters the light experienced by the phytoplankton, with stronger mixing potentially disrupting light sufficiently to hinder photosynthesis. The net effect, i.e., whether or not the extra mixing aids net phytoplankton production, will depend on some balance between the nutrient and light effects. The summer reduction in bottom water oxygen concentrations will also respond to the increased mixing. Oxygen will be supplied from the surface water downward, potentially offsetting some of the normal bacterial demand for oxygen as they recycle the sinking organic detritus from phytoplankton growth. At the same time, however, there may be an increased supply of organic detrital material if the net effect of mixing on primary production was positive, in which case the bacterial demand for oxygen in the bottom water will increase. Understanding the net effect of mixing on bottom water is important, as there are large areas of stratified shelf seas that are currently viewed as being close to experiencing oxygen depletion in late summer (Ciavatta et al., 2016).

Changes to biogeochemical functioning would need to be assessed over several years. For instance, an immediate positive impact on net phytoplankton production because of the extra nutrient supply will mean that the total amount of the water column inventory of nutrients used for that year will have increased. The shelf is not restocked with fresh nutrients from the open ocean every year (Ruiz-Castillo et al., 2019), so the ability of the shelf system to maintain the increased production will depend on how efficient the system is at recycling organic nutrients back to inorganic nutrients particularly over the winter.

A natural analog to the effects of renewable energy infrastructure in a stratified environment may be found in the central Celtic Sea, where a number of seabed banks interact with tidal flows to inject significant internal wave-driven mixing into the thermocline (Palmer et al., 2013). While the exact biogeochemical and biological reasons are not yet clear, it does appear that the bank-driven mixing increases the overall biological activity of the region, ultimately resulting in commercial fishing (see, e.g., **Figures 1C**, **4** Sharples et al., 2013). The island mixing effect too (Simpson et al., 1982), produces significantly enhanced nutrient fluxes, with a corresponding increase in plankton production and fishing activity. Thus, combined with reduced fishing pressure, appropriate infrastructure in suitable locations could prove a positive impact on regional ecology, with benefits to wildlife and fisheries.

The changes in the timing of stratification expected from increases in mixing also need to be considered. Late development of stratification and the spring bloom has the potential to impact wildlife, which has evolved to take advantage of this abundance, with seabird breeding populations and fish stocks a notable risk. At the other end of the stratified period, additional mixing will lead to earlier re-mixing of the whole water column, shortening the total productive time of the area and also altering the timing of the autumn bloom. Similarly, some seabird colonies are located to take advantage of the enhanced productivity at tidal mixing fronts (Trevail et al., 2019), the location of which may be affected by additional mixing from offshore wind farm infrastructure.

4.4. Management and Mitigation Requirements

Environmental Impact Assessments (EIA) are required for all new offshore wind farms to mitigate negative impacts resulting from construction, operation and decommissioning across the lifecycle of use. Surveying also covers geophysical site assessment, focus on seabed composition, current assessments and the potential for seabed scour around anchors and cables. Current EIAs have been developed for mixed coastal environments to ensure sustainable growth of the offshore wind sector. Beyond the construction phase, impact has been focused on the benthic habitat and individual species interactions with infrastructure. Impact on marine mammals, seabird colonies, and fisheries in the region are individually assessed, but without consideration of potential alteration of the primary production through enhanced mixing.

To ensure the continued growth of the sector (The Crown Estate, 2020), impacts of the new generation of developments in deeper seasonally stratified regimes will likely require a more fundamental assessment. Baseline surveys must include the natural cycle of water column stratification, biogeochemical

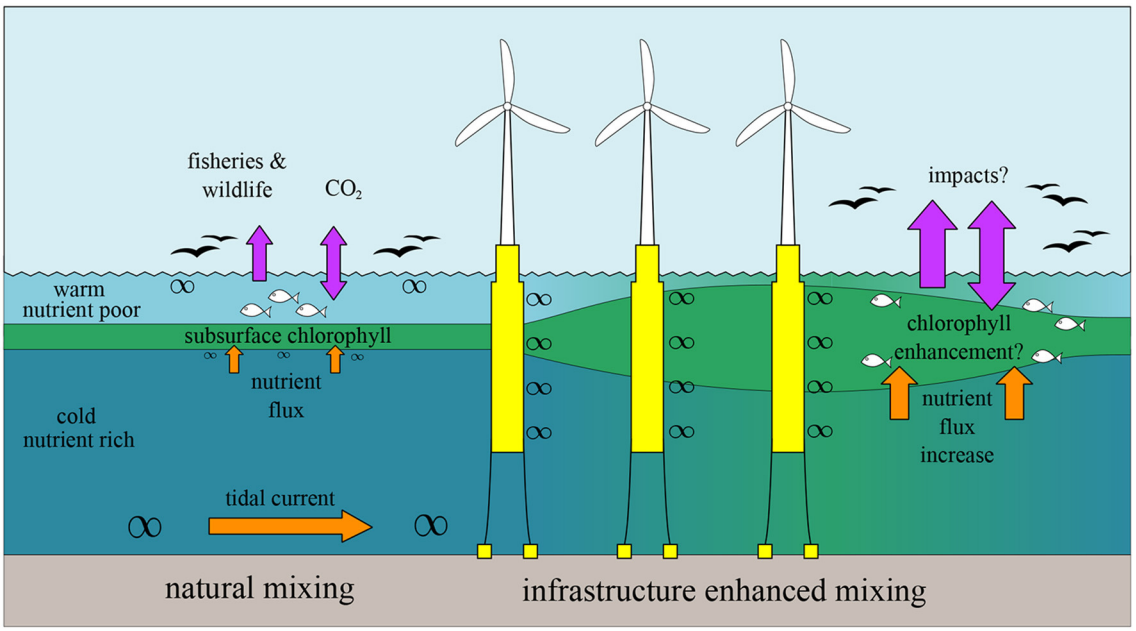

FIGURE 14 | Offshore wind infrastructure adds wake turbulence throughout the upper water column, including directly at the thermocline. Here swirl size indicates turbulence intensity arising from near bed, near surface and flow-structure induced shear. Wake turbulence mixes cold nutrient rich bottom water with warm nutrient poor surface water, reducing the strength of stratification and potentially enhancing plankton growth in the subsurface chlorophyll layer. Changes in the subsurface chlorophyll layer would have further impacts on nutrient pathways, ecosystem functioning and oceanic carbon sequestration.

fluxes, and primary production. Accurately forecasting the interaction between the flow, infrastructure and stratification will require site, array and design specific observations and model scenarios. Only with a comprehensive understanding of this physical modification to the biogeochemical functioning of shelf seas, can impact throughout the marine web be adequately assessed.

5. CONCLUSIONS

Previous work has considered the environmental impact that offshore wind energy has on well-mixed shallow-water marine ecosystems, including from benthic habits, fisheries to seabirds. Much of this work remains relevant to enable sector growth. However, sector expansion from well-mixed shallow water to seasonally stratified deeper water represents a fundamental change, where physical and environmental impacts are not understood.

For the first time planned developments of both fixed and floating offshore wind infrastructure will add large scale anthropogenic mixing to seasonally stratified shelf seas. Large scale mixing may force shelf sea physics, establishing a 'new normal' for biogeochemical cycles and shelf sea ecosystem functioning. The potential benefits and risks posed by infrastructure mixing of stratified shelf seas, on top of climate change, represents a combined hazard that has not been considered.

Locally, flow past offshore wind energy infrastructure results in (barotropic) drag and turbulence that, by itself, dissipates at least 140% more energy than exists naturally at the thermocline (Section 3.3). However, in stratified waters, the additional baroclinic (wave) drag can exceed the barotropic drag. For example, the baroclinic drag for a stratified flow past topography can be 1–2 magnitudes larger than the barotropic drag (Smith, 1978). Baroclinic drag from vertical infrastructure in stratified flow, such as OWT, is as yet unquantified. Moreover, the role of horizontal shear on vertical mixing, here produced by obstacles that scale with density gradient length scales, is poorly understood, particularly in complex stratifications like the thermocline. It is of great importance to extend our understanding of the fundamental fluid dynamics of flows past vertical structures in ocean-realistic stratifications, in particular, the onset of turbulence and ensuing mixing associated with the breakdown of induced vortices.

Regionally, the first order paradigm for seasonally stratified shelf seas is the balance between the stratifying influence of surface heating, and the input of mechanical energy to mix the water column at the upper and lower boundaries (due to wind stress and the tidal shear, respectively). High resolution shelf sea models have some success in reproducing this (Luneva et al., 2019). However, the addition of mixing from large scale offshore wind farm development, limits our ability to understand the trajectory of shelf sea ecosystems. To address this, research is urgently needed that scales processes from: a single turbine; an array of turbines composing a wind farm; to an entire shelf sea region with multiple farms. Advances in regional ecosystem

modeling must then be validated against direct before-and-after observations to skillfully assess the direct and indirect impacts of anthropogenic mixing, and so guide sustainable development.

Growth of the offshore wind energy industry must be accelerated to meet global 2050 Net Zero commitments. Risks posed by offshore wind development in stratified shelf seas should be mitigated against, but potential benefits should be identified and maximized. Research should consider how nature based solutions, foundation design and array layout can enable sector growth, mitigation of risks and maximization of benefits.

AUTHOR CONTRIBUTIONS

RD wrote and coordinated contributions to the article. CL wrote section Flow Structure Interactions and contributed to sections Introduction, Oceanography of Stratification in Shelf Seas, Discussion, and Conclusions. BL wrote section Oceanography of Stratification in Shelf Seas and contributed to sections Discussion and Conclusions. TR and JHS contributed to sections Oceanography of Stratification in Shelf Seas Discussion, and Conclusions. JT and JP contributed to sections Oceanography of Stratification in Shelf Seas, Flow Structure Interactions, Discussion, and Conclusions. C-cC contributed to sections Flow Structure Interactions, Discussion, and Conclusions. JS contributed to sections Oceanography of Stratification in Shelf Seas and Discussion. BS contributed to section Oceanography of Stratification in Shelf Seas. DG contributed to sections Introduction and Discussion. RH contributed to sections Introduction, Oceanography of Stratification in Shelf Seas, Flow Structure Interactions, Discussion, and Conclusions. All authors reviewed the entire manuscript.

FUNDING

RD acknowledges the support of the UK Natural Environment Research Council NE/S014535/1. CL acknowledges the support of the Offshore Renewable Energy Catapult. BL acknowledges the support of the Smart Efficient Energy Centre, Bangor University, part funded by the European Regional Development Fund. DG acknowledges the support of the UK Engineering and Physical Sciences Research Council EP/S000747/1. JP acknowledges the support of the Natural Environment Research Council Climate Linked Atlantic Sector Science (CLASS) programme.

REFERENCES

4C Offshore (2021). *Global Offshore Renewable Map*. Available online at: https://www.4coffshore.com/offshorewind (accessed September 30, 2021).

Arntsen, Ø. A. (1996). Disturbances, lift and drag forces due to the translation of a horizontal circular cylinder in stratified water. *Exp. Fluids* 21, 387–400. doi: 10.1007/BF00189060

Augier, P., Billant, P., and Chomaz, J.-M. (2015). Stratified turbulence forced with columnar dipoles: numerical study. *J. Fluid Mech.* 769, 403–443. doi: 10.1017/jfm.2015.76

Austin, J. A., and Barth, J. A. (2002). Variation in the position of the upwelling front on the oregon shelf. *J. Geophys. Res. Oceans* 107, 1–1. doi: 10.1029/2001JC000858

Basak, S., and Sarkar, S. (2006). Dynamics of a stratified shear layer with horizontal shear. *J. Fluid Mech.* 568, 19–54. doi: 10.1017/S0022112006001686

Bauer, J. E., Cai, W.-J., Raymond, P. A., Bianchi, T. S., Hopkinson, C. S., and Regnier, P. A. (2013). The changing carbon cycle of the coastal ocean. *Nature* 504, 61–70. doi: 10.1038/nature12857

Billant, P., and Chomaz, J.-M. (2000a). Experimental evidence for a new instability of a vertical columnar vortex pair in a strongly stratified fluid. *J. Fluid Mech.* 418, 167–188. doi: 10.1017/S0022112000001154

Billant, P., and Chomaz, J.-M. (2000b). Theoretical analysis of the zigzag instability of a vertical columnar vortex pair in a strongly stratified fluid. *J. Fluid Mech.* 419, 29–63. doi: 10.1017/S0022112000001166

Bluteau, C., Jones, N., and Ivey, G. (2013). Turbulent mixing efficiency at an energetic ocean site. *J. Geophys. Res. Oceans* 118, 4662–4672. doi: 10.1002/jgrc.20292

Bosco, M., and Meunier, P. (2014). Three-dimensional instabilities of a stratified cylinder wake. *J. Fluid Mech.* 759, 149–180. doi: 10.1017/jfm.2014.517

Boyer, D., Davies, P., Fernando, H., and Zhang, X. (1989). Linearly stratified flow past a horizontal circular cylinder. *Philos. Trans. R. Soc. Lond. A Math. Phys. Sci.* 328, 501–528. doi: 10.1098/rsta.1989.0049

Broström, G. (2008). On the influence of large wind farms on the upper ocean circulation. *J. Mar. Syst.* 74, 585–591. doi: 10.1016/j.jmarsys.2008.05.001

Burchard, H., and Rippeth, T. P. (2009). Generation of bulk shear spikes in shallow stratified tidal seas. *J. Phys. Oceanogr.* 39, 969–985. doi: 10.1175/2008JPO4074.1

Butterfield, S., Musial, W., Jonkman, J., and Sclavounos, P. (2007). *Engineering Challenges for Floating Offshore Wind Turbines*. Technical report, National Renewable Energy Lab. (NREL), Golden, CO.

Carpenter, J. R., Merckelbach, L., Callies, U., Clark, S., Gaslikova, L., and Baschek, B. (2016). Potential impacts of offshore wind farms on north sea stratification. *PLoS ONE* 11, e0160830. doi: 10.1371/journal.pone.0160830

Castro, I., Snyder, W., and Baines, P. (1990). Obstacle drag in stratified flow. *Proc. R. Soc. Lond. A Math. Phys. Sci.* 429, 119–140. doi: 10.1098/rspa.1990.0054

Castro-Santos, L., Silva, D., Bento, A. R., Salvacao, N., and Soares, C. G. (2020). Economic feasibility of floating offshore wind farms in portugal. *Ocean Eng.* 207, 107393. doi: 10.1016/j.oceaneng.2020.107393

Caulfield, C. (2021). Layering, instabilities, and mixing in turbulent stratified flows. *Annu. Rev. Fluid Mech.* 53, 113–145. doi: 10.1146/annurev-fluid-042320-100458

Cazenave, P. W., Torres, R., and Allen, J. I. (2016). Unstructured grid modelling of offshore wind farm impacts on seasonally stratified shelf seas. *Prog Oceanogr.* 145, 25–41. doi: 10.1016/j.pocean.2016.04.004

Ciavatta, S., Kay, S., Saux-Picart, S., Butenschön, M., and Allen, J. (2016). Decadal reanalysis of biogeochemical indicators and fluxes in the north west european shelf-sea ecosystem. *J. Geophys. Res. Oceans* 121, 1824–1845. doi: 10.1002/2015JC011496

Cimbala, J. M., and Krein, M. V. (1990). Effect of freestream conditions on the far wake of a circular cylinder. *AIAA J.* 28, 1369–1373. doi: 10.2514/3.25227

Cocetta, F., Gillard, M., Szmelter, J., and Smolarkiewicz, P. K. (2021). Stratified flow past a sphere at moderate reynolds numbers. *Comput. Fluids* 226, 104998. doi: 10.1016/j.compfluid.2021.104998

Cottura, L., Caradonna, R., Ghigo, A., Novo, R., Bracco, G., and Mattiazzo, G. (2021). Dynamic modeling of an offshore floating wind turbine for application in the mediterranean sea. *Energies* 14, 248. doi: 10.3390/en14010248

Cummins, P. F., Topham, D. R., and Pite, H. D. (1994). Simulated and experimental two-layer flows past isolated two-dimensional obstacles. *Fluid Dyn. Res.* 14, 105. doi: 10.1016/0169-5983(94)90055-8

Dalziel, S. B., Patterson, M. D., Caulfield, C., and Le Brun, S. (2011). The structure of low-froude-number lee waves over an isolated obstacle. *J. Fluid Mech.* 689, 3–31. doi: 10.1017/jfm.2011.384

Dannheim, J., Bergström, L., Birchenough, S. N., Brzana, R., Boon, A. R., Coolen, J. W., et al. (2020). Benthic effects of offshore renewables: identification of knowledge gaps and urgently needed research. *ICES J. Mar. Sci.* 77, 1092–1108. doi: 10.1093/icesjms/fsz018

Deloncle, A., Billant, P., and Chomaz, J.-M. (2008). Nonlinear evolution of the zigzag instability in stratified fluids: a shortcut on the route to dissipation. *J. Fluid Mech.* 599, 229–239. doi: 10.1017/S0022112007000109

Díaz, H., and Soares, C. G. (2020). Review of the current status, technology and future trends of offshore wind farms. *Ocean Eng.* 209, 107381. doi: 10.1016/j.oceaneng.2020.107381

Eames, I., Jonsson, C., and Johnson, P. (2011). The growth of a cylinder wake in turbulent flow. *J. Turbulence* 12:N39. doi: 10.1080/14685248.2011.619985

Egbert, G., and Ray, R. (2000). Significant dissipation of tidal energy in the deep ocean inferred from satellite altimeter data. *Nature* 405, 775–778. doi: 10.1038/35015531

Egbert, G. D., and Erofeeva, S. Y. (2002). Efficient inverse modeling of barotropic ocean tides. *J. Atmosphere. Oceanic Technol.* 19, 183–204. doi: 10.1175/1520-0426(2002)019andlt;0183:EIMOBOandgt;2.0.CO;2

Esteban, M. D., Diez, J. J., López, J. S., and Negro, V. (2011). Why offshore wind energy? *Renew Energy* 36, 444–450. doi: 10.1016/j.renene.2010.07.009

Esteban, M. D., López-Gutiérrez, J.-S., and Negro, V. (2019). Gravity-based foundations in the offshore wind sector. *J. Mar. Sci. Eng.* 7, 64. doi: 10.3390/jmse7030064

Exo, K.-M., Huppop, O., and Garthe, S. (2003). Birds and offshore wind farms: a hot topic in marine ecology. *Bull. Wader Study Group* 100, 50–53. Available online at: https://sora.unm.edu/node/121708

Floeter, J., van Beusekom, J. E., Auch, D., Callies, U., Carpenter, J., Dudeck, T., et al. (2017). Pelagic effects of offshore wind farm foundations in the stratified north sea. *Prog. Oceanogr.* 156, 154–173. doi: 10.1016/j.pocean.2017.07.003

Forster, R. M. (2018). *The effect of monopile-induced turbulence on local suspended sediment patterns around uk wind farms: field survey report*. Technical report, An IECS report to The Crown Estate, IECS, University of Hull, Hull, HU6 7RX. ISBN=978-1-906410-77-3.

Frederiksen, M., Edwards, M., Richardson, A. J., Halliday, N. C., and Wanless, S. (2006). From plankton to top predators: bottom-up control of a marine food web across four trophic levels. *J. Anim. Ecol.* 75, 1259–1268. doi: 10.1111/j.1365-2656.2006.01148.x

Garrett, C., Keeley, J., and Greenberg, D. (1978). Tidal mixing versus thermal stratification in the bay of fundy and gulf of maine. *Atmosphere Ocean* 16, 403–423. doi: 10.1080/07055900.1978.9649046

Ghosal, S., and Rogers, M. M. (1997). A numerical study of self-similarity in a turbulent plane wake using large-eddy simulation. *Phys. Fluids* 9, 1729–1739. doi: 10.1063/1.869289

Global Wind Energy Council. (2020). *Global Offshore Wind Report*. Available online at: https://gwec.net/global-offshore-wind-report-2020/ (accessed August 8, 2021).

Glorioso, P. D., and Flather, R. A. (1995). A barotropic model of the currents off se south america. *J. Geophys. Res. Oceans* 100, 13427–13440. doi: 10.1029/95JC00942

Golbraikh, E., and Beegle-Krause, C. (2020). A model for the estimation of the mixing zone behind large sea vessels. *Environ. Sci. Pollut. Res.* 27, 37911–37919. doi: 10.1007/s11356-020-09890-y

Gowen, R., Stewart, B., Mills, D., and Elliott, P. (1995). Regional differences in stratification and its effect on phytoplankton production and biomass in the northwestern irish sea. *J. Plankton Res.* 17, 753–769. doi: 10.1093/plankt/17.4.753

Graham, J. A., O'Dea, E., Holt, J., Polton, J., Hewitt, H. T., Furner, R., et al. (2018). Amm15: a new high-resolution nemo configuration for operational simulation of the european north-west shelf. *Geosci. Model Dev.* 11, 681–696. doi: 10.5194/gmd-11-681-2018

Grashorn, S., and Stanev, E. V. (2016). Kármán vortex and turbulent wake generation by wind park piles. *Ocean Dyn.* 66, 1543–1557. doi: 10.1007/s10236-016-0995-2

Gray, T., Haggett, C., and Bell, D. (2005). Offshore wind farms and commercial fisheries in the uk: a study in stakeholder consultation. *Ethics Place Environ.* 8, 127–140. doi: 10.1080/13668790500237013

Guihou, K., Polton, J., Harle, J., Wakelin, S., O'Dea, E., and Holt, J. (2018). Kilometric scale modeling of the north west european shelf seas: Exploring the spatial and temporal variability of internal tides. *J. Geophys. Res. Oceans* 123, 688–707. doi: 10.1002/2017JC012960

Gula, J., Molemaker, M., and McWilliams, J. (2015). Topographic vorticity generation, submesoscale instability and vortex street formation in the gulf stream. *Geophys. Res. Lett.* 42, 4054–4062. doi: 10.1002/2015GL063731

Gula, J., Taylor, J., Shcherbina, A., and Mahadevan, A. (2022). "Submesoscale processes and mixing," in *Ocean Mixing: Drivers, Mechanisms and Impacts*, eds M. Meredith and A. N. Garabato (Elsevier), 181–214. doi: 10.1016/B978-0-12-821512-8.00015-3

Hewitt, G., Vassilicos, C., et al. (2005). *Prediction of Turbulent Flows*. Cambridge: Cambridge University Press.

Holt, J., and Proctor, R. (2008). The seasonal circulation and volume transport on the northwest european continental shelf: a fine-resolution model study. *J. Geophys. Res. Oceans* 113:C6. doi: 10.1029/2006JC004034

Howard, L. N. (1961). Note on a paper of john w. miles. *J. Fluid Mech.* 10, 509–512. doi: 10.1017/S0022112061000317

Howland, M. F., Lele, S. K., and Dabiri, J. O. (2019). Wind farm power optimization through wake steering. *Proc. Natl. Acad. Sci. U.S.A.* 116, 14495–14500. doi: 10.1073/pnas.1903680116

Inall, M. E., Rippeth, T. P., and Sherwin, T. J. (2000). Impact of nonlinear waves on the dissipation of internal tidal energy at a shelf break. *J. Geophys. Res. Oceans* 105, 8687–8705. doi: 10.1029/1999JC900299

Inall, M. E., Toberman, M., Polton, J. A., Palmer, M. R., Green, J. M., and Rippeth, T. P. (2021). Shelf seas baroclinic energy loss: pycnocline mixing and bottom boundary layer dissipation. *J. Geophys. Res. Oceans* 126, e2020JC016528. doi: 10.1029/2020JC016528

Jacobsen, A., and Godvik, M. (2021). Influence of wakes and atmospheric stability on the floater responses of the hywind scotland wind turbines. *Wind Energy* 24, 149–161. doi: 10.1002/we.2563

Jacobsen, H. K., Hevia-Koch, P., and Wolter, C. (2019). Nearshore and offshore wind development: costs and competitive advantage exemplified by nearshore wind in denmark. *Energy Sustain. Dev.* 50, 91–100. doi: 10.1016/j.esd.2019.03.006

Jansen, M., Staffell, I., Kitzing, L., Quoilin, S., Wiggelinkhuizen, E., Bulder, B., et al. (2020). Offshore wind competitiveness in mature markets without subsidy. *Nat. Energy* 5, 614–622. doi: 10.1038/s41560-020-0661-2

Jiang, H. (2021a). Formation mechanism of a secondary vortex street in a cylinder wake. *J. Fluid Mech.* 915,A127. doi: 10.1017/jfm.2021.195

Jiang, H., and Cheng, L. (2019). Transition to the secondary vortex street in the wake of a circular cylinder. *J. Fluid Mech.* 867, 691–722. doi: 10.1017/jfm.2019.167

Jiang, Z. (2021b). Installation of offshore wind turbines: a technical review. *Renew. Sustain. Energy Rev.* 139, 110576. doi: 10.1016/j.rser.2020.110576

Khani, S., and Waite, M. L. (2015). Large eddy simulations of stratified turbulence: the dynamic smagorinsky model. *J. Fluid Mech.* 773, 327–344. doi: 10.1017/jfm.2015.249

Komori, S., Nagaosa, R., and Murakami, Y. (1993). Turbulence structure and mass transfer across a sheared air-water interface in wind-driven turbulence. *J. Fluid Mech.* 249, 161–183. doi: 10.1017/S0022112093001120

Kröger, S., Parker, R., Cripps, G., and Williamson, P. (2018). *Shelf Seas: The Engine of Productivity, Policy Report on NERC-Defra Shelf Sea Biogeochemistry Programme*. Lowesoft: Cefas. doi: 10.14465/2018.ssb18.pbd

Lévy, M., Ferrari, R., Franks, P. J., Martin, A. P., and Rivière, P. (2012). Bringing physics to life at the submesoscale. *Geophys. Res. Lett.* 39. doi: 10.1029/2012GL052756

Lévy, M., Klein, P., and Treguier, A.-M. (2001). Impact of sub-mesoscale physics on production and subduction of phytoplankton in an oligotrophic regime. *J. Mar. Res.* 59, 535–565. doi: 10.1357/002224001762842181

Lie, H.-J. (1989). Tidal fronts in the southeastern hwanghae (yellow sea). *Cont. Shelf Res.* 9, 527–546. doi: 10.1016/0278-4343(89)90019-8

Lienhard, J. H., et al. (1966). *Synopsis of lift, drag, and vortex frequency data for rigid circular cylinders, Vol. 300*. Technical Extension Service, Washington State University Pullman, WA.

Lincoln, B., Rippeth, T., and Simpson, J. (2016). Surface mixed layer deepening through wind shear alignment in a seasonally stratified shallow sea. *J. Geophys. Res. Oceans* 121, 6021–6034. doi: 10.1002/2015JC011382

Loder, J. W., and Greenberg, D. A. (1986). Predicted positions of tidal fronts in the gulf of maine region. *Cont. Shelf Res.* 6, 397–414. doi: 10.1016/0278-4343(86)90080-4

Lucas, D., Caulfield, C., and Kerswell, R. (2017). Layer formation in horizontally forced stratified turbulence: connecting exact coherent structures to linear instabilities. *J. Fluid Mech.* 832, 409–437. doi: 10.1017/jfm.2017.661

Lucas, N. S., Grant, A. L., Rippeth, T. P., Polton, J. A., Palmer, M. R., Brannigan, L., et al. (2019). Evolution of oceanic near-surface stratification in response to an autumn storm. *J. Phys. Oceanogr.* 49, 2961–2978. doi: 10.1175/JPO-D-19-0007.1

Luneva, M. V., Wakelin, S., Holt, J. T., Inall, M. E., Kozlov, I. E., Palmer, M. R., et al. (2019). Challenging vertical turbulence mixing schemes in a tidally energetic environment: 1. 3-d shelf-sea model assessment. *J. Geophys. Res. Oceans* 124, 6360–6387. doi: 10.1029/2018JC014307

Maffioli, A., Davidson, P., Dalziel, S., and Swaminathan, N. (2014). The evolution of a stratified turbulent cloud. *J. Fluid Mech.* 739, 229–253. doi: 10.1017/jfm.2013.612

Mahadevan, A. (2016). The impact of submesoscale physics on primary productivity of plankton. *Ann. Re.v Mar. Sci.* 8, 161–184. doi: 10.1146/annurev-marine-010814-015912

Mahadevan, A., and Archer, D. (2000). Modeling the impact of fronts and mesoscale circulation on the nutrient supply and biogeochemistry of the upper ocean. *J. Geophys. Res. Oceans* 105, 1209–1225. doi: 10.1029/1999JC900216

Mahadevan, A., D'asaro, E., Lee, C., and Perry, M. J. (2012). Eddy-driven stratification initiates north atlantic spring phytoplankton blooms. *Science* 337, 54–58. doi: 10.1126/science.1218740

Mahadevan, A., and Tandon, A. (2006). An analysis of mechanisms for submesoscale vertical motion at ocean fronts. *Ocean Model.* 14, 241–256. doi: 10.1016/j.ocemod.2006.05.006

Mahaffey, C., Palmer, M., Greenwood, N., and Sharples, J. (2020). Impacts of climate change on dissolved oxygen concentration relevant to the coastal and marine environment around the uk. *MCCIP Sci. Rev.* 2002, 31–53. doi: 10.14465/2020.arc02.oxy

Marmorino, G. O., Smith, G. B., North, R. P., and Baschek, B. (2018). Application of airborne infrared remote sensing to the study of ocean submesoscale eddies. *Front. Mech. Eng.* 4, 10. doi: 10.3389/fmech.2018.00010

Matutano, C., Negro, V., López-Gutiérrez, J.-S., and Esteban, M. D. (2013). Scour prediction and scour protections in offshore wind farms. *Renew. Energy* 57, 358–365. doi: 10.1016/j.renene.2013.01.048

McWilliams, J. C. (2016). Submesoscale currents in the ocean. *Proc. R. Soc. A Math. Phys. Eng. Sci.* 472, 20160117. doi: 10.1098/rspa.2016.0117

Meunier, P. (2012). Stratified wake of a tilted cylinder. part 1. suppression of a von kármán vortex street. *J. Fluid Mech.* 699, 174–197. doi: 10.1017/jfm.2012.92

Miles, J. W. (1961). On the stability of heterogeneous shear flows. *J. Fluid Mech.* 10, 496–508. doi: 10.1017/S0022112061000305

Molemaker, M. J., McWilliams, J. C., and Dewar, W. K. (2015). Submesoscale instability and generation of mesoscale anticyclones near a separation of the california undercurrent. *J. Phys. Oceanogr.* 45, 613–629. doi: 10.1175/JPO-D-13-0225.1

Monismith, S. G., Koseff, J. R., and White, B. L. (2018). Mixing efficiency in the presence of stratification: when is it constant? *Geophys. Res. Lett.* 45, 5627–5634. doi: 10.1029/2018GL077229

Nakamura, N. (1996). Two-dimensional mixing, edge formation, and permeability diagnosed in an area coordinate. *J. Atmospher. Sci.* 53, 1524–1537. doi: 10.1175/1520-0469(1996)053andlt;1524:TDMEFAandgt;2.0.CO;2

Nygaard, N. G., Steen, S. T., Poulsen, L., and Pedersen, J. G. (2020). Modelling cluster wakes and wind farm blockage. *J. Phys.* 1618, 062072. doi: 10.1088/1742-6596/1618/6/062072

Nylund, A. T., Arneborg, L., Tengberg, A., Mallast, U., and Hassellöv, I.-M. (2020). *In situ* observations of turbulent ship wakes and their potential implications for vertical mixing. *Ocean Sci. Discuss.* 17, 1285–1302. doi: 10.5194/os-2020-59

Oakey, N. S., and Greenan, B. J. (2004). Mixing in a coastal environment: 2. a view from microstructure measurements. *J. Geophys. Res. Oceans* 109:C10. doi: 10.1029/2003JC002193

Offshore Renewable Energy Action Coalition (2020). *The Power of Our Ocean Report*. Available online at: https://gwec.net/oreac/ (accessed August 15, 2021).

Omand, M. M., D'Asaro, E. A., Lee, C. M., Perry, M. J., Briggs, N., Cetinić, I., et al. (2015). Eddy-driven subduction exports particulate organic carbon from the spring bloom. *Science* 348, 222–225. doi: 10.1126/science.1260062

Ouellet, P., Fuentes-Yaco, C., Savard, L., Platt, T., Sathyendranath, S., Koeller, P., et al. (2011). Ocean surface characteristics influence recruitment variability of populations of northern shrimp (pandalus borealis) in the northwest atlantic. *ICES J. Mar. Sci.* 68, 737–744. doi: 10.1093/icesjms/fsq174

Palmer, M. R., Polton, J. A., Inall, M. E., Rippeth, T. P., Green, J. A. M., Sharples, J., et al. (2013). Variable behavior in pycnocline mixing over shelf seas. *Geophys. Res. Lett.* 40, 1–6. doi: 10.1029/2012GL054638

Palmer, M. R., Rippeth, T. P., and Simpson, J. H. (2008). An investigation of internal mixing in a seasonally stratified shelf sea. *J. Geophys. Res. Oceans* 113, 1–14. doi: 10.1029/2007JC004531

Paskyabi, M. B., and Fer, I. (2012). Upper ocean response to large wind farm effect in the presence of surface gravity waves. *Energy Procedia* 24, 245–254. doi: 10.1016/j.egypro.2012.06.106

Pauly, D., Christensen, V., Guénette, S., Pitcher, T. J., Sumaila, U. R., Walters, C. J., et al. (2002). Towards sustainability in world fisheries. *Nature* 418, 689–695. doi: 10.1038/nature01017

Pearson, B. C., Grant, A. L. M., Polton, J. A., and Belcher, S. E. (2015). Langmuir turbulence and surface heating in the ocean surface boundary layer. *J. Phys. Oceanogr.* 45, 2897–2911. doi: 10.1175/JPO-D-15-0018.1

Pingree, R., and Griffiths, D. (1978). Tidal fronts on the shelf seas around the british isles. *J. Geophys. Res. Oceans* 83, 4615–4622. doi: 10.1029/JC083iC09p04615

Pingree, R., Mardell, G., Holligan, P., Griffiths, D., and Smithers, J. (1982). Celtic sea and armorican current structure and the vertical distributions of temperature and chlorophyll. *Cont. Shelf Res.* 1, 99–116. doi: 10.1016/0278-4343(82)90033-4

Platt, T., Fuentes-Yaco, C., and Frank, K. T. (2003). Spring algal bloom and larval fish survival. *Nature* 423, 398–399. doi: 10.1038/423398b

Polton, J., Smith, J., MacKinnon, J., and Tejada-Martínez, A. (2008). Rapid generation of high-frequency internal waves beneath a wind and wave forced oceanic surface mixed-layer. *Geophys. Res. Lett.* 35, L13602. doi: 10.1029/2008GL033856

Ren, S., Xie, J., and Zhu, J. (2014). The roles of different mechanisms related to the tide-induced fronts in the yellow sea in summer. *Adv. Atmosphere. Sci.* 31, 1079–1089. doi: 10.1007/s00376-014-3236-y

Rennau, H., Schimmels, S., and Burchard, H. (2012). On the effect of structure-induced resistance and mixing on inflows into the baltic sea: a numerical model study. *Coastal Eng.* 60, 53–68. doi: 10.1016/j.coastaleng.2011.08.002

Richardson, K., Visser, A., and Pedersen, F. B. (2000). Subsurface phytoplankton blooms fuel pelagic production in the north sea. *J. Plankton Res.* 22, 1663–1671. doi: 10.1093/plankt/22.9.1663

Rippeth, T. P. (2005). Mixing in seasonally stratified shelf seas: a shifting paradigm. *Philos. Trans. R. Soc. A Math. Phys. Eng. Sci.* 363, 2837–2854. doi: 10.1098/rsta.2005.1662

Rippeth, T. P., Palmer, M. R., Simpson, J. H., Fisher, N. R., and Sharples, J. (2005). Thermocline mixing in summer stratified continental shelf seas. *Geophys. Res. Lett.* 32, 4. doi: 10.1029/2004GL022104

Rippeth, T. P., Wiles, P., Palmer, M. R., Sharples, J., and Tweddle, J. (2009). The diapcynal nutrient flux and shear-induced diapcynal mixing in the seasonally stratified western irish sea. *Cont. Shelf Res.* 29, 1580–1587. doi: 10.1016/j.csr.2009.04.009

Roobaert, A., Laruelle, G. G., Landschützer, P., Gruber, N., Chou, L., and Regnier, P. (2019). The spatiotemporal dynamics of the sources and sinks of co2 in the global coastal ocean. *Global Biogeochem. Cycles* 33, 1693–1714. doi: 10.1029/2019GB006239

Ruiz-Castillo, E., Sharples, J., Hopkins, J., and Woodward, M. (2019). Seasonality in the cross-shelf physical structure of a temperate shelf sea and the implications for nitrate supply. *Prog. Oceanogr.* 177, 101985. doi: 10.1016/j.pocean.2018.07.006

Scannell, B. (2020). *Developing the Structure Function Method for Evaluating Turbulent Kinetic Energy Dissipation Rate* (Ph.D. thesis), Bangor, Wales, UK.

Scannell, B. D., Lenn, Y.-D., and Rippeth, T. P. (2021). Impact of adcp motion on structure function estimates of turbulent kinetic energy dissipation rate. *Ocean Sci. Discuss.* 2021, 1–38. doi: 10.5194/os-2021-71

Schneider, J. A., and Senders, M. (2010). Foundation design: a comparison of oil and gas platforms with offshore wind turbines. *Mar. Technol. Soc. J.* 44, 32–51. doi: 10.4031/MTSJ.44.1.5

Schultze, L., Merckelbach, L., Horstmann, J., Raasch, S., and Carpenter, J. (2020a). Increased mixing and turbulence in the wake of offshore wind farm foundations. *J. Geophys. Res. Oceans* 125, e2019JC015858. doi: 10.1029/2019JC015858

Schultze, L., Merckelbach, L. M., and Carpenter, J. R. (2020b). "Towed chain datasets and input files for simulations used in the manuscript "Increased mixing and turbulence in the wake of offshore wind farm foundations". *J. Geophys. Res. Oceans* 125, e2019JC015858.

Schumacher, J., Kinder, T., Pashinski, D., and Charnell, R. (1979). A structural front over the continental shelf of the eastern bering sea. *J. Phys. Oceanogr.* 9, 79–87. doi: 10.1175/1520-0485(1979)009andlt;0079:ASFOTCandgt;2.0.CO;2

Sharples, J., Ellis, J. R., Nolan, G., and Scott, B. E. (2013). Fishing and the oceanography of a stratified shelf sea. *Progr. Oceanogr.* 117, 130–139. doi: 10.1016/j.pocean.2013.06.014

Sharples, J., Moore, C. M., and Abraham, E. R. (2001a). Internal tide dissipation, mixing, and vertical nitrate flux at the shelf edge of ne new zealand. *J. Geophys. Res. Oceans* 106, 14069–14081. doi: 10.1029/2000JC000604

Sharples, J., Moore, M. C., Rippeth, T. P., Holligan, P. M., Hydes, D. J., Fisher, N. R., et al. (2001b). Phytoplankton distribution and survival in the thermocline. *Limnol. Oceanogr.* 46, 486–496. doi: 10.4319/lo.2001.46.3.0486

Sharples, J., and Tett, P. (1994). Modelling the effect of physical variability on the midwater chlorophyll maximum. *J Mar. Res.* 52, 219–238. doi: 10.1357/0022240943077109

Sharples, J., Tweddle, J. F., Mattias Green, J., Palmer, M. R., Kim, Y.-N., Hickman, A. E., et al. (2007). Spring-neap modulation of internal tide mixing and vertical nitrate fluxes at a shelf edge in summer. *Limnol. Oceanogr.* 52, 1735–1747. doi: 10.4319/lo.2007.52.5.1735

Sheehan, P. M., Berx, B., Gallego, A., Hall, R. A., Heywood, K. J., Hughes, S. L., et al. (2018). Shelf sea tidal currents and mixing fronts determined from ocean glider observations. *Ocean Sci.* 14, 225–236. doi: 10.5194/os-14-225-2018

Shen, W., Chen, X., Qiu, J., Hayward, J. A., Sayeef, S., Osman, P., et al. (2020). A comprehensive review of variable renewable energy levelized cost of electricity. *Renew. Sustain. Energy Rev.* 133, 110301. doi: 10.1016/j.rser.2020.110301

Silvester, J. M., Lenn, Y.-D., Polton, J. A., Rippeth, T. P., and Maqueda, M. M. (2014). Observations of a diapycnal shortcut to adiabatic upwelling of antarctic circumpolar deep water. *Geophys. Res. Lett.* 41, 7950–7956. doi: 10.1002/2014GL061538

Simpson, J., Allen, C., and Morris, N. (1978). Fronts on the continental shelf. *J. Geophys. Res. Oceans* 83, 4607–4614. doi: 10.1029/JC083iC09p04607

Simpson, J., and Bowers, D. (1981). Models of stratification and frontal movement in shelf seas. *Deep Sea Res. A Oceanogr. Res. Pap.* 28, 727–738. doi: 10.1016/0198-0149(81)90132-1

Simpson, J., and Hunter, J. (1974). Fronts in the irish sea. *Nature* 250, 404–406. doi: 10.1038/250404a0

Simpson, J., Tett, P., Argote-Espinoza, M., Edwards, A., Jones, K., and Savidge, G. (1982). Mixing and phytoplankton growth around an island in a stratified sea. *Cont. Shelf Res.* 1, 15–31. doi: 10.1016/0278-4343(82)90030-9

Simpson, J. H., Crawford, W. R., Rippeth, T. P., Campbell, A. R., and Cheok, J. V. (1996). The vertical structure of turbulent dissipation in shelf seas. *J. Phys. Oceanogr.* 26, 1579–1590. doi: 10.1175/1520-0485(1996)026andlt;1579:TVSOTDandgt;2.0.CO;2

Simpson, J. H., and Sharples, J. (2012). *Introduction to the Physical and Biological Oceanography of Shelf Seas*. Cambridge: Cambridge University Press.

Smith, R. B. (1978). A measurement of mountain drag. *J. Atmosphere. Sci.* 35, 1644–1654. doi: 10.1175/1520-0469(1978)035<1644:AMOMD>2.0.CO;2

Soares-Ramos, E. P., de Oliveira-Assis, L., Sarrias-Mena, R., and Fernández-Ramírez, L. M. (2020). Current status and future trends of offshore wind power in europe. *Energy* 202, 117787. doi: 10.1016/j.energy.2020.117787

Srinivasan, K., McWilliams, J. C., Molemaker, M. J., and Barkan, R. (2019). Submesoscale vortical wakes in the lee of topography. *J. Phys. Oceanogr.* 49, 1949–1971. doi: 10.1175/JPO-D-18-0042.1

Stigebrandt, A., and Aure, J. (1989). Vertical mixing in basin waters of fjords. *J. Physical Oceanogr.* 19, 917–926. doi: 10.1175/1520-0485(1989)019andlt;0917:VMIBWOandgt;2.0.CO;2

Sun, X., Huang, D., and Wu, G. (2012). The current state of offshore wind energy technology development. *Energy* 41, 298–312. doi: 10.1016/j.energy.2012.02.054

Taylor, J., and Zhou, Q. (2017). A multi-parameter criterion for layer formation in a stratified shear flow using sorted buoyancy coordinates. *J. Fluid Mech.* 823, R5. doi: 10.1017/jfm.2017.375

Taylor, J. R. (2016). Turbulent mixing, restratification, and phytoplankton growth at a submesoscale eddy. *Geophys. Res. Lett.* 43, 5784–5792. doi: 10.1002/2016GL069106

Taylor, J. R., and Ferrari, R. (2011). Ocean fronts trigger high latitude phytoplankton blooms. *Geophys. Res. Lett.* 38, 5. doi: 10.1029/2011GL049312

Taylor, J. R., Smith, K. M., and Vreugdenhil, C. A. (2020). The influence of submesoscales and vertical mixing on the export of sinking tracers in large-eddy simulations. *J. Phys. Oceanogr.* 50, 1319–1339. doi: 10.1175/JPO-D-19-0267.1

The Crown Estate (2020). *BROAD HORIZONS: Key Resource Areas for Offshore Wind Summary Report*. Available online at: https://www.thecrownestate.co.uk/media/3642/broad-horizons-offshore-wind-key-resource-area-summary-report.pdf (accessed December 5, 2021).

Thomas, H., Bozec, Y., Elkalay, K., and De Baar, H. J. (2004). Enhanced open ocean storage of co2 from shelf sea pumping. *Science* 304, 1005–1008. doi: 10.1126/science.1095491

Thomas, L. N., Tandon, A., and Mahadevan, A. (2008). Submesoscale processes and dynamics. *Ocean Model. Eddying Regime* 177, 17–38. doi: 10.1029/177GM04

Thorpe, S. (2016). Layers and internal waves in uniformly stratified fluids stirred by vertical grids. *J. Fluid Mech.* 793, 380–413. doi: 10.1017/jfm.2016.121

Tonani, M., Sykes, P., King, R. R., McConnell, N., Pquignet, A.-C., O'Dea, E., et al. (2019). The impact of a new high-resolution ocean model on the met office north-west european shelf forecasting system. *Ocean Sci.* 15, 1133–1158. doi: 10.5194/os-15-1133-2019

Tong, J., Gan, Z., Qi, Y., and Mao, Q. (2010). Predicted positions of tidal fronts in continental shelf of south china sea. *J. Mar. Syst.* 82, 145–153. doi: 10.1016/j.jmarsys.2010.04.011

Trevail, A. M., Green, J. A., Sharples, J., Polton, J. A., Arnould, J. P. Y., and Patrick, S. C. (2019). Environmental heterogeneity amplifies behavioural response to a temporal cycle. *Oikos* 128, 517–528. doi: 10.1111/oik.05579

Umlauf, L., and Burchard, H. (2005). Second-order turbulence closure models for geophysical boundary layers. a review of recent work. *Continental Shelf Res.* 25, 795–827. doi: 10.1016/j.csr.2004.08.004

United Nations (2015). *Sustainable Development Goals*. Available online at: https://sdgs.un.org/goals (accessed August 15, 2021).

Uzunoglu, E., and Soares, C. G. (2020). Hydrodynamic design of a free-float capable tension leg platform for a 10 mw wind turbine. *Ocean Eng.* 197, 106888. doi: 10.1016/j.oceaneng.2019.106888

van Berkel, J., Burchard, H., Christensen, A., Mortensen, L. O., Petersen, O. S., and Thomsen, F. (2020). The effects of offshore wind farms on hydrodynamics and implications for fishes. *Oceanography* 33, 108–117. doi: 10.5670/oceanog.2020.410

van Haren, H., Maas, L., Zimmerman, J., Ridderinkhof, H., and Malschaert, H. (1999). Strong inertial currents and marginal internal wave stability in the central north sea. *Geophys Res Lett.* 26, 2993–2996. doi: 10.1029/1999GL002352

Vindenes, H., Orvik, K. A., Søiland, H., and Wehde, H. (2018). Analysis of tidal currents in the north sea from shipboard acoustic doppler current profiler data. *Cont. Shelf Res.* 162, 1–12. doi: 10.1016/j.csr.2018.04.001

Waite, M., and Smolarkiewicz, P. (2008). Instability and breakdown of a vertical vortex pair in a strongly stratified fluid. *J. Fluid Mech.* 606, 1–35. doi: 10.1017/S0022112008001912

Wen, C., Dallimer, M., Carver, S., and Ziv, G. (2018). Valuing the visual impact of wind farms: A calculus method for synthesizing choice experiments studies. *Sci. Total Environ.* 637, 58–68. doi: 10.1016/j.scitotenv.2018.04.430

Weston, K., Fernand, L., Mills, D., Delahunty, R., and Brown, J. (2005). Primary production in the deep chlorophyll maximum of the central north sea. *J. Plankton Res.* 27, 909–922. doi: 10.1093/plankt/fbi064

Williams, C., Sharples, J., Green, M., Mahaffey, C., and Rippeth, T. (2013a). The maintenance of the subsurface chlorophyll maximum in the stratified western irish sea. *Limnol. Oceanogr. Fluids Environ.* 3, 61–73. doi: 10.1215/21573689-2285100

Williams, C., Sharples, J., Mahaffey, C., and Rippeth, T. (2013b). Wind-driven nutrient pulses to the subsurface chlorophyll maximum in seasonally stratified shelf seas. *Geophys. Res. Lett*. 40, 5467–5472. doi: 10.1002/2013GL058171

Williamson, C., and Prasad, A. (1993). A new mechanism for oblique wave resonance in the natural far wake. *J. Fluid Mech*. 256, 269–313. doi: 10.1017/S0022112093002794

Williamson, C. H. (1996). Vortex dynamics in the cylinder wake. *Annu. Rev. Fluid Mech*. 28, 477–539. doi: 10.1146/annurev.fl.28.010196.002401

Winters, K. B., and D'Asaro, E. A. (1996). Diascalar flux and the rate of fluid mixing. *J. Fluid Mech*. 317, 179–193. doi: 10.1017/S0022112096000717

Wollast, R. (1998). Evaluation and comparison of the global carbon cycle in the coastal zone and in the open ocean. *Sea* 10, 213–252.

Xu, W., Liu, Y., Wu, W., Dong, Y., Lu, W., Liu, Y., et al. (2020). Proliferation of offshore wind farms in the north sea and surrounding waters revealed by satellite image time series. *Renew. Sustain. Energy Rev*. 133, 110167. doi: 10.1016/j.rser.2020.110167

Zhou, Q., Taylor, J., Caulfield, C., and Linden, P. (2017). Diapycnal mixing in layered stratified plane couette flow quantified in a tracer-based coordinate. *J. Fluid Mech*. 823, 198–229. doi: 10.1017/jfm.2017.261

Conflict of Interest: The authors declare that the research was conducted in the absence of any commercial or financial relationships that could be construed as a potential conflict of interest.